

There and back again: understanding the critical properties of backsplash galaxies

Josh Borrow,^{1*} Mark Vogelsberger,¹ Stephanie O’Neil,¹ Michael A. McDonald¹ and Aaron Smith^{1†}

¹*Department of Physics and Kavli Institute for Astrophysics and Space Research, Massachusetts Institute of Technology, Cambridge, MA 02139, USA*

Accepted XXX. Received YYY; in original form ZZZ

ABSTRACT

Backsplash galaxies are galaxies that once resided inside a cluster, and have migrated back outside as they move towards the apocentre of their orbit. The kinematic properties of these galaxies are well understood, thanks to the significant study of back-splashers in dark matter-only simulations, but their intrinsic properties are not well constrained due to modelling uncertainties in sub-grid physics, ram pressure stripping, dynamical friction, and tidal forces. In this paper, we use the IllustrisTNG300-1 simulation, with a baryonic resolution of $M_b \approx 1.1 \times 10^7 M_\odot$, to study backsplash galaxies around 1302 isolated galaxy clusters with mass $10^{13.0} < M_{200,\text{mean}}/M_\odot < 10^{15.5}$. We employ a decision tree classifier to extract features of galaxies that make them likely to be backsplash galaxies, compared to nearby field galaxies, and find that backsplash galaxies have low gas fractions, high mass-to-light ratios, large stellar sizes, and low black hole occupation fractions. We investigate in detail the origins of these large sizes, and hypothesise their origins are linked to the tidal environments in the cluster. We show that the black hole recentring scheme employed in many cosmological simulations leads to the loss of black holes from galaxies accreted into clusters, and suggest improvements to these models. Generally, we find that backsplash galaxies are a useful population to test and understand numerical galaxy formation models due to their challenging environments and evolutionary pathways that interact with poorly constrained physics.

Key words: galaxies: clusters: general, galaxies: interactions, galaxies: formation, galaxies: evolution, galaxies: kinematics and dynamics

1 INTRODUCTION

Understanding the assembly and composition of galaxy clusters has been a topic of research for decades. Within the Lambda-CDM cosmological paradigm, these massive systems are understood to be hierarchically created from many smaller substructures. Galaxy clusters are assembled when many subhaloes, containing galaxies, accrete together to form self-bound structures of halo mass $M_{200,\text{mean}} > 10^{13} M_\odot$. Here $M_{200,\text{mean}}$ is defined as the mass enclosed within $R_{200,\text{mean}}$, the radius enclosing 200 times the mean density of the Universe at that epoch. What happens when one of these galaxies leaves the cluster again? Is such a process possible? If so, what do these galaxies look like and why? This paper explores the life and times of such ‘backsplash’ galaxies, through the use of the TNG300 cosmological galaxy formation simulation, and attempts to address these open questions.

Backsplash galaxies were first studied in early theoretical work by Balogh et al. (2000), using mass accretion histories from N-body simulations and an analytical model to explain star formation gradients in the outskirts of galaxy clusters. The general understanding was that galaxy clusters quench galaxies, and galaxies that fall into clusters have a chance of ‘bouncing’ back out of the clusters to

an apocentre greater than the virial radius R_{vir} , provided they have enough orbital energy. Hence, in the outskirts of the clusters, star forming galaxies would be mixed with these quenched backsplash galaxies, with the number of backsplashes dropping off with radius but the density of the infalling population remaining relatively constant with radius, giving rise to a gradient in star formation activity even further out than R_{vir} .

This early work was complimented by theoretical and observational studies by Mamon et al. (2004) and Sanchis et al. (2004) looking at neutral hydrogen (HI) deficient galaxies near the Virgo cluster. It was not until Gill et al. (2005), however, that the term ‘backsplash galaxy’ was actually coined, which was the first systematic study evaluating the expected kinematic (i.e. including velocity-space information) properties of these interlopers. Gill et al. (2005) used N-body simulations to predict that 50% of galaxies in the range $1 < R/R_{\text{vir}} < 2$ would be backsplash galaxies, and that these galaxies had close pericentre passages to the centre of the cluster before rebounding. Within a month, Kilborn et al. (2005) provided observational evidence of two HI-poor galaxies within this radial range around the NGC 1566 group, further suggesting that such galaxies could indeed exist in the real Universe.

Later theoretical and observational work by Ludlow et al. (2009), Hansen et al. (2009), Knebe et al. (2011), and Bahé et al. (2013), using a variety of techniques, cemented the idea that backsplash galaxies are a cause of colour gradients in galaxies out to multiple times

* E-mail: josh@joshborrow.com, borrowj@mit.edu (JB)

† NHFP Einstein Fellow.

$R_{200,\text{mean}}$. Notably, Knebe et al. (2011) found that the processing and production of backplash subhaloes even occurs on dwarf galaxy scales, in simulations of the local group.

Much of the work investigating the interaction of cluster galaxies and their hosts has employed the use of semi-analytical models, which use a base dark matter-only simulation to generate accretion histories, followed by an analytical model for studying the baryonic component. Simulating galaxy clusters with a full hydrodynamical treatment is incredibly complex, with authors turning to zoom simulations (where only a small fraction of the volume is hydrodynamically active), or sacrificing numerical resolution significantly (Barnes et al. 2017; McCarthy et al. 2017; Ragone-Figueroa et al. 2018; Haggar et al. 2020; Bassini et al. 2020). Additionally, the processes involved in the evolution and production of backplash galaxies, including ram-pressure stripping and dynamical friction, are still not fully understood (Simpson et al. 2018; van den Bosch & Ogiya 2018). The subhaloes that are able to rebound from the cluster are typically of lower mass, with subhaloes with total halo mass $M_{\text{H}}/M_{200,\text{mean}} > 0.01$ strongly impacted by dynamical friction leading to rapid merging with the central galaxy in the cluster (Bakels et al. 2021).

Despite these potential numerical pitfalls, there has recently been renewed interest in backplash galaxies as a potential formation mechanism of ultra-diffuse galaxies (UDGs, see e.g. van Dokkum et al. 2015; Koda et al. 2015; Tremmel et al. 2020; Jones et al. 2021). UDGs are low surface-brightness dwarf galaxies, typically with larger stellar sizes than field dwarfs. Many UDGs are located near clusters and have intrinsic properties similar to those expected of backplash galaxies (Benavides et al. 2021; Trujillo 2021). Additionally, the challenges of simulating backplash galaxies make them an excellent testing ground for the accuracy of numerical models. Modern galaxy formation models are currently able to reproduce a statistically representative sample of simulated galaxies, but typically struggle to reproduce the observed properties of ‘extremophile’ galaxies that reside in extreme environments (Somerville & Davé 2015; Vogelsberger et al. 2020; de los Rios et al. 2021).

Recently, Farid et al. (2022) used a random forest algorithm to classify the membership properties of cluster galaxies, and was able to perform such classification with high ($> 80\%$) accuracy when employing phase-space information. In practice, however, phase-space information is difficult to generate as typically only velocities along the line of sight (from redshift information) can be observed. To reach this accuracy, they additionally augment their model by using the specific star formation rate (sSFR) of galaxies, but a notable inaccuracy in their model is that they underpredict the classification of orbiting galaxies at radii $1.0 < R/R_{200,\text{mean}} < 2.0$ (i.e. their model underclassifies backplash galaxies) when using a hard classification scheme.

In this paper, we aim to classify galaxies near clusters into two categories, infalling (never within $R_{200,\text{mean}}$ of a cluster), and backplash (has been within $R_{200,\text{mean}}$ of a cluster, but are now further away). We use the IllustrisTNG suite of cosmological galaxy formation simulations, and employ the largest volume simulation with a comoving box-size of $(300\text{Mpc})^3$. Through the development of a classification model for the galaxies based upon their intrinsic properties, we aim to identify which features of backplash galaxies make them unique from the general field population, and use these features to understand their formation and evolution.

The rest of this paper is organised as follows: In §2, we give a brief overview of the IllustrisTNG model and simulations. In §3, we describe our cluster and galaxy selection process, and discuss some basic properties of backplash galaxies in the TNG model. In §4,

we use a decision tree machine learning model to understand which properties of galaxies can be used to classify them as backplashers or infalling. In §5, we discuss the origins of the larger sizes of backplash galaxies, and in §6, we aim to understand the low supermassive black hole occupation fraction and masses in backplash galaxies. Finally, in §7, we give concluding remarks.

2 THE ILLUSTRISTNG SIMULATION SUITE

In this work we use simulations from the IllustrisTNG suite of cosmological galaxy formation simulations, released in Nelson et al. (2019). In particular, we use data from the public release of the IllustrisTNG300-1 simulation (Pillepich et al. 2018b; Springel et al. 2018; Nelson et al. 2018; Naiman et al. 2018; Marinacci et al. 2018). The simulation is henceforth referred to as TNG300, and follows a $(300\text{Mpc})^3$ comoving, representative, volume of universe from just after the big bang down to the present day at $z = 0$. All results in this paper should be assumed to be at $z = 0$ unless otherwise stated.

The TNG300 volume initially contains 2500^3 gas cells of target mass $1.1 \times 10^7 M_{\odot}$ and 2500^3 dark matter particles of fixed mass $5.9 \times 10^7 M_{\odot}$. These particles are evolved over cosmic time using the continuum magnetohydrodynamics (MHD) and gravity code AREPO (Springel 2011; Weinberger et al. 2020). AREPO is a massively parallel code that uses a moving Voronoi mesh coupled with a finite volume method to compute forces and fluxes originating from MHD, along with a combined tree and particle mesh (TreePM) method to calculate periodic and non-periodic self-gravitational forces.

Coupled to the base AREPO code is the IllustrisTNG galaxy formation sub-grid model, a successor to the Illustris galaxy formation model (Vogelsberger et al. 2013, 2014b). Galaxy formation sub-grid models are required to include physics that occurs below the resolution scale. Within the TNG model, there are prescriptions for radiative gas cooling (Wiersma et al. 2009), star formation and stellar feedback (Springel & Hernquist 2003), and (supermassive) black hole formation and active galactic nuclei feedback (Weinberger et al. 2017). The simulation was performed assuming a cosmology conforming to the 2015 release from the Planck satellite, with $\Omega_{\Lambda,0} = 0.6911$, $\Omega_{\text{m},0} = 0.3089$, $\Omega_{\text{b},0} = 0.0486$, $\sigma_8 = 0.8159$, $n_s = 0.9667$, and $h = 0.6774$, with the symbols having their usual meaning (Planck Collaboration et al. 2016). More information on the specific implementation details is available in the data release paper and associated webpages (Nelson et al. 2019).

Here we primarily use reduced data from the available SUBFIND group catalogues. SUBFIND primarily uses a friends-of-friends (FoF) algorithm (Springel et al. 2005; Dolag et al. 2009) to identify haloes and their constituent subhaloes. In TNG300, the initial FoF search uses a typical default linking length of $b = 0.2$, before the SUBFIND galaxy finder algorithm is ran. For each of the 100 TNG300 snapshots, a group catalogue is created containing properties of galaxies (subhaloes) and groups (haloes). These group catalogues are used, along with the L-HALOTREE algorithm (Springel et al. 2005), to follow the paths of individual structures over time and build up a merger tree of haloes.

3 SELECTING BACKSPASH GALAXIES

As we were motivated to study backplash galaxies by the study of the splashback radius of galaxy clusters, we use the same sample of clusters as in O’Neil et al. (2022). These are chosen to be isolated

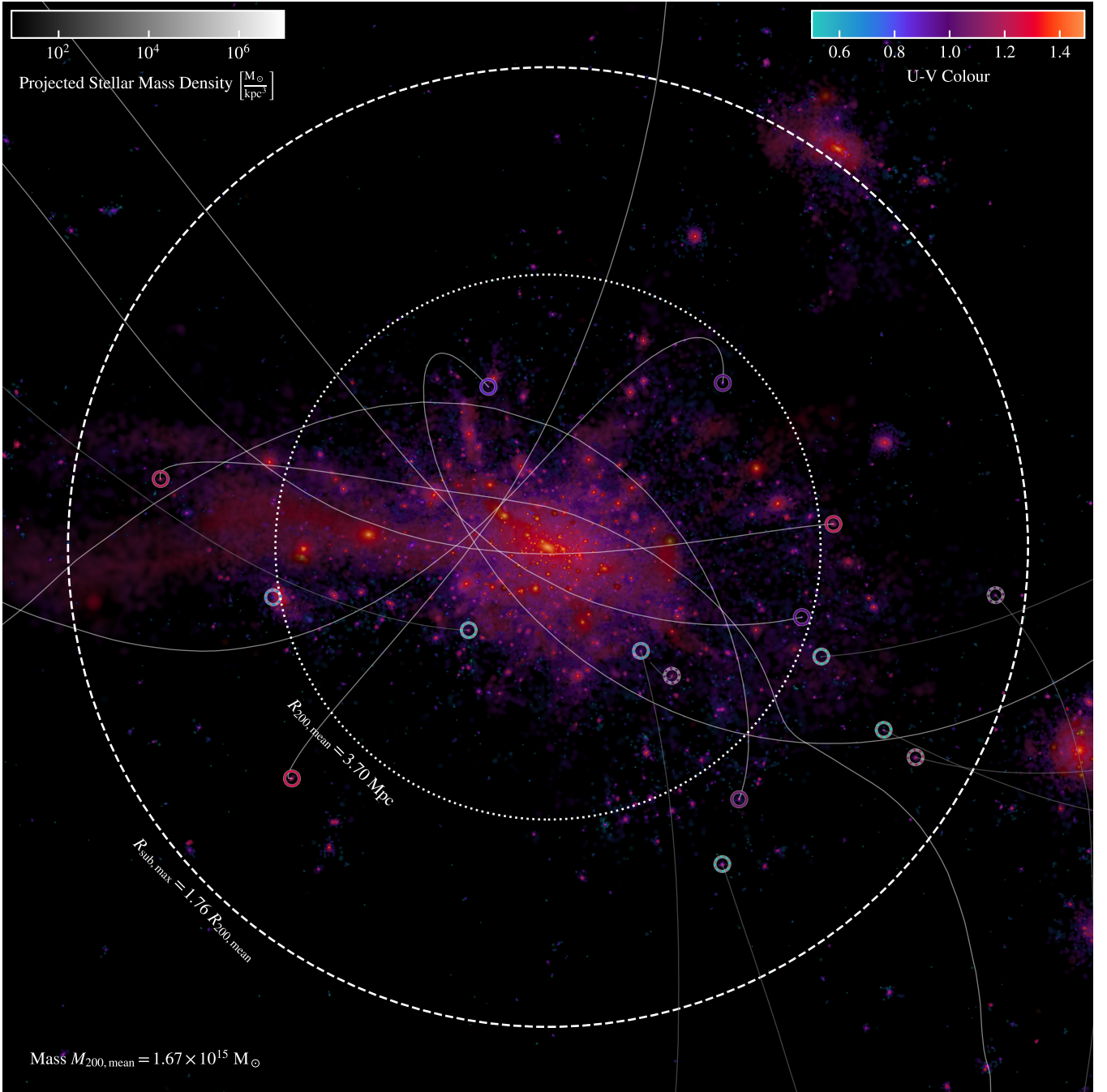


Figure 1. Shows a $10^{15} M_{\odot}$ cluster from the Illustris TNG300 simulation. The background image shows the stellar density (luminance of the image; i.e. brighter regions have a higher projected stellar density), with the colour showing the mean, mass-weighted, $U - V$ colour along the line of sight. Each ring shows a galaxy that currently resides outside the radius $R_{200,\text{mean}}$ (dotted white line), with the rings coloured by the $U - V$ colour of the substructure. If the ring is dotted, it represents an infalling galaxy (note that these are typically bluer), and if solid it is a backsplash galaxy. The white dashed line shows the maximal (3D) radius that a backsplash substructure can be found at for this cluster ($R_{\text{sub,max}}$). Finally, the thin light lines show the paths of the highlighted galaxies.

galaxy clusters with a mass $M_{200,\text{mean}} > 10^{13} M_{\odot}$. This sample is constructed by ensuring that the clusters are the most massive within $10R_{200,\text{mean}}$ of any nearby cluster. This is ensured by, for every candidate in the $z = 0$ snapshot, looping over all other candidates within $10R_{200,\text{mean}}$. In this loop, if any nearby candidate has a mass lower than the cluster being considered, it is marked as removed from the sample.

The advantage of this approach (as compared to only looping over

nearby members and asserting there must be no halo of greater mass) is that if, say, there is a $M_{200,\text{mean}} = 10^{13} M_{\odot}$ galaxy cluster near a $M_{200,\text{mean}} = 10^{15} M_{\odot}$ cluster, the lower mass one (which will be significantly impacted by the nearby, more massive, cluster, despite the $10^{13} M_{\odot}$ cluster not ‘seeing’ the $10^{15} M_{\odot}$ cluster in its radial search) is not included in our sample.

For each isolated cluster we then employ the L-HALOTREE merger trees, and track the first progenitor (most massive subhalo)

of the cluster back in time. To ensure that we are able to accurately track the movement of the cluster back in time (and as such reconstruct the paths of its satellites accurately), we apply an additional set of constraints:

- The first progenitor of the cluster must be traceable through at least the most recent 40 snapshots (at least back to $z = 0.7$, or approximately half a Hubble time). This ensures we have a stable enough cluster to follow infalling galaxies for at least a handful of cluster crossing times (typically $t_{\text{cross}} \approx 1 - 2$ Gyr).
- The cluster must not move more than 10 Mpc per Gyr (comoving) relative to the fixed box, to ensure that it corresponds to the local potential maximum. This works alongside our isolated galaxy constraint to ensure that as few as possible backplash galaxies are transferred between clusters and experience interactions with more than one cluster. In particular, this could skew our results since galaxies that have passed through a different cluster would not be identified as backplash despite being subject to a cluster environment similar to backplash galaxies of its current host halo.
- In a similar fashion, there must be less than a 0.5 Mpc offset between where the cluster is predicted to be based upon its velocity and time between snapshots relative to its position in the next snapshot.

This set of constraints ensures that the clusters move smoothly, and are the most dominant halo within their local neighborhood, to ensure a clean sample of infalling and backsplashing galaxies. The final selection of clusters rejects around 100 compared to O’Neil et al. (2022), with 1302 clusters remaining.

To track the galaxies resident in, and near, these clusters, we again employ the L-HALOTREE merger trees. We identify all galaxies within the range $1 < R_{200,\text{mean}} < 10$ of each cluster at $z = 0$, and track their first progenitor (whether it is bound to, enters, or is associated with the merger tree of the cluster or not) back as far as it can be identified by the tree. We apply a stellar mass cut of $M_* > 10^8 M_\odot$, only tracking substructure that has a mass higher than this at $z = 0$ back in time, to ensure that all substructure would be visible and to ease computational load, though such a tracking procedure is not particularly computationally complex.

We then assign galaxies a label of ‘backplash’ or ‘infalling’ based on whether they have come within $R_{200,\text{mean}}$ of the cluster (at the relevant redshift) at any time. In Fig. 1, we show the tracks of some example backplash and infalling galaxies, alongside a massive galaxy cluster ($M_{200,\text{mean}} = 1.67 \times 10^{15} M_\odot$). The infalling galaxies, indicated by dotted circles, have yet to interact with the cluster (note that this is a projection along the z -axis of the simulation), whereas the backplash galaxies (indicated by solid rings) have had a close periapsis with the cluster. Notable in this image is the dense prescence of galaxies on the opposing side of the cluster to the infalling filament (on the left of the image). We also identify the maximal radius at which any backsplashing substructure is found at, $R_{\text{sub,max}}$.

From Fig. 1 it is clear that we expect some divergence in the properties of backplash and infalling galaxies. It is already clear that the infalling galaxies are much bluer, with backplash galaxies being red (i.e. a high $U - V$ colour).

Fig. 2 shows some basic properties of backplash galaxies as they scale with the cluster mass $M_{200,\text{mean}}$. The top panel shows the fraction of all subhaloes within the range $1 < R/R_{200,\text{mean}} < 2$ that are backplashers, which is consistently around 30% across the cluster mass range. Our backplash fraction is lower than previously studied simulations, with Gill et al. (2005) finding a backplash fraction of 50%, and Hagggar et al. (2020) finding that the backplash

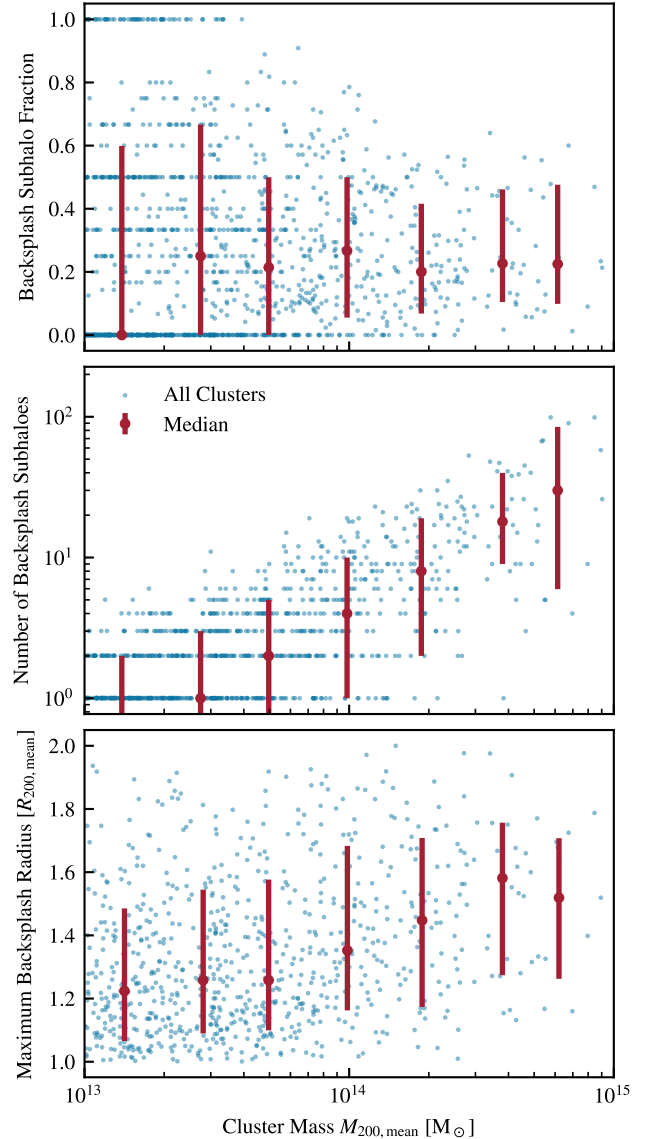


Figure 2. Shows properties of backplash galaxies as a function of host cluster mass. In all panels, the blue dots represent the position of a single cluster in the plane, with the red error bars showing the 16th, 50th, and 84th percentile ranges (bottom, point, top) for clusters binned in 8 equally log-spaced bins between $10^{13} \leq M_{200,\text{mean}}/M_\odot \leq 10^{15}$. *Top panel:* The fraction of subhaloes in the range $1.0 < R/R_{200,\text{mean}} < 2.0$ that are classified as backplash galaxies. *Middle panel:* The total number of backplash galaxies within this range as a function of cluster mass. This only edges above a median of one in clusters with $M_{200,\text{mean}} > 10^{13.5} M_\odot$. *Bottom panel:* The maximum radius at which a backplash galaxy is found for all clusters.

fraction is of order 60%. Hagggar et al. (2020) uses significantly higher mass clusters ($5 \times 10^{14} < M_{200,\text{crit}}/M_\odot < 3 \times 10^{15}$) than this work, and apply a much higher mass cut on their galaxies (with $M_* > 10^{9.5} M_\odot$). Additionally, they find that the backplash fraction depends on the relaxation of the cluster, with the most relaxed clusters having backplash fractions less than 20%. Our isolation and tracking criteria for our clusters, required as they live in live, full volume simulations (as opposed to zoom-in simulations of clusters like THETHREEHUNDRED sample), likely selects more relaxed clusters. As we are mainly interested in the properties of the back-

splash galaxies themselves, rather than their host clusters, we defer further investigation to potential future work.

The central panel shows that below cluster masses of $M_{200,\text{mean}} = 10^{14} M_{\odot}$, a very low fraction of clusters have any backsplash galaxies at all, and the number of backsplash subhaloes scales roughly linearly with cluster mass. This is primarily due to two factors: their smaller values of $R_{200,\text{mean}}$ leading to a smaller volume within which backsplash galaxies may reside, and their lower density environments.

Finally, the bottom panel of Fig. 2 shows the distribution of the maximal radii at which backsplash subhaloes are found ($R_{\text{sub,max}}$ in Fig. 1). In this panel, clusters are not included if they do not have any backsplash subhaloes. We find that the maximal radius, relative to $R_{200,\text{mean}}$, increases with cluster mass. This is particularly notable as the splashback radius R_{sp} has been shown by many authors, in particular O’Neil et al. (2021) for this sample, to decrease with cluster mass. Typical values of the splashback radius are roughly $R_{\text{sp}}/R_{200,\text{mean}} \approx 1.1 - 1.2$, as measured based upon the dark matter profiles, trending down with cluster mass. That there are many galaxies outside of the typical splashback radius for these clusters is not particularly surprising; the splashback radius should be the point at which backsplash galaxies and infalling galaxies are at rough equipartition (assuming galaxy number density traces mass density). We attribute the increase in maximal backsplash galaxy radius with mass to the better sampling that these haloes have, with them simply being more likely to find a galaxy out at this radius.

Fig. 3 shows the radial number density profile of galaxies, stacked across all clusters in our sample, and rescaled by $R_{200,\text{mean}}$. Even by $R = 1.1R_{200,\text{mean}}$, galaxies that are infalling become more abundant, indicating just how rare backsplash galaxies are. We indicate that within the annulus of $1.0 < R/R_{200,\text{mean}} < 1.24$ the density of backsplash galaxies and infalling galaxies are equal. Bakels et al. (2021) finds that the radius at which backsplashing and infalling subhaloes have equal density is at around $R/R_{200,\text{crit}} \approx 1.8$ (their Fig. 3)¹, similar to our $R/R_{200,\text{mean}} \approx 1.1$, making our results consistent despite their more complex tracking procedure. We find little evolution in the equipartition radius with host cluster mass, with it placed at $R/R_{200,\text{mean}} = 1.26$ and 1.24 for clusters in mass ranges $10^{13} < M_{200,\text{mean}}/M_{\odot} < 10^{14}$ and $10^{14} < M_{200,\text{mean}}/M_{\odot} < 10^{15}$ respectively, and hence only show the stacked profile across our entire cluster sample.

Fig. 3 shows that the infalling component has a near-constant density across the radial range, with the backsplash (orbital) component falling off rapidly with radius. This suggests that looking for galaxies bound to the cluster much further away than $R/R_{200,\text{mean}} \approx 1.5$ is unlikely to yield a large number of results. Further, it suggests that galaxies found this far away are unlikely to have been processed by the cluster previously, meaning that in all likelihood their properties are determined by their internal evolution rather than their environment.

In Fig. 4 we show the radial velocity distributions of the cluster galaxies in our sample, split by host cluster halo mass. Here we calculate radial velocity disregarding the negligible Hubble flow component (of order 100 km s^{-1}) to better understand the gravitational dynamics at play in clusters. This becomes non-negligible for the highest mass clusters that host galaxies at the largest radii in the lower panels, meaning that there is an offset in the central velocity for backsplash galaxies. The radial velocity is calculated in the

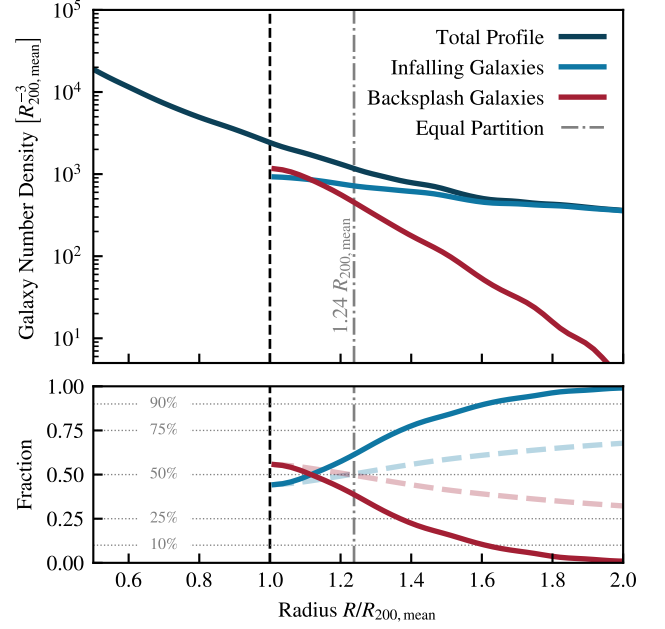


Figure 3. *Top panel:* The number density profile of all galaxies with $M_* > 10^8 M_{\odot}$ in our sample, stacked for all clusters in the sample. The dark blue line shows the profile of all galaxies, with the vertical black dashed line delineating the point at which backsplash galaxies are classified ($R_{200,\text{mean}}$). Outside this radius, the infalling galaxies (light blue) and backsplash galaxies (red) have their profiles shown separately, with the infalling galaxies tracing an almost constant density, and the density of the backsplash galaxies falling off rapidly outside of the cluster. *Bottom Panel:* The volume-weighted fraction of backsplash and infalling galaxies as a function of radius. Horizontal dotted lines are shown at common percentile ranges to guide the eye. By $1.6R_{200,\text{mean}}$ fewer than 10% of galaxies are backsplash, making attempts to classify galaxies outside this radius infeasible. The dashed, lighter, lines shown in the background show the cumulative fraction of galaxies in each classification out to this radius (i.e. the fraction of galaxies with radius $r < R$ that are backsplash or infalling galaxies). The equal partition between these two classifications is reached at $1.24R_{200,\text{mean}}$ (grey dot-dash line)

rest frame of the cluster and is given by

$$v_r = \frac{(\vec{v}_{\text{gal}} - \vec{v}_{\text{clu}}) \cdot (\vec{x}_{\text{gal}} - \vec{x}_{\text{clu}})}{|\vec{x}_{\text{gal}} - \vec{x}_{\text{clu}}|}, \quad (1)$$

where here \vec{v} and \vec{x} are the physical velocity and position of the cluster and galaxy (subscripts clu and gal respectively) relative to the simulation box.

We see that the velocities of backsplash galaxies generally follow a normal distribution around zero, with roughly equal numbers of galaxies on their way out ($v_r > 0$) as in ($v_r < 0$) to the cluster. The infalling galaxies, on the other hand, almost universally are falling into the cluster ($v_r < 0$, note that we did not make a velocity-based cut in our criterion for infalling galaxies, just that they must be near a cluster and not have been in the cluster previously). In almost all cases, the absolute value of the velocity for backsplash galaxies is significantly lower than the velocity of infalling galaxies. The infalling galaxies have a mean velocity that scales with the cluster mass, with higher mass clusters having significantly faster infall speeds ($v_r \approx -250 \text{ km s}^{-1}$ for $10^{13.0} < M_{200,\text{mean}}/M_{\odot} \leq 10^{13.5}$ clusters, versus $v_r \approx -1100 \text{ km s}^{-1}$ for $10^{15.0} < M_{200,\text{mean}}/M_{\odot} \leq 10^{15.5}$ clusters). The higher infall velocities of galaxies in high mass clusters is a potential explanation for the increase of $R_{\text{sub,max}}$ with mass seen in the bottom panel of Fig. 2.

¹ We remind readers that ratios of $R_{200,\text{mean}}/R_{200,\text{crit}} \approx 1.65$ are typical for cluster haloes.

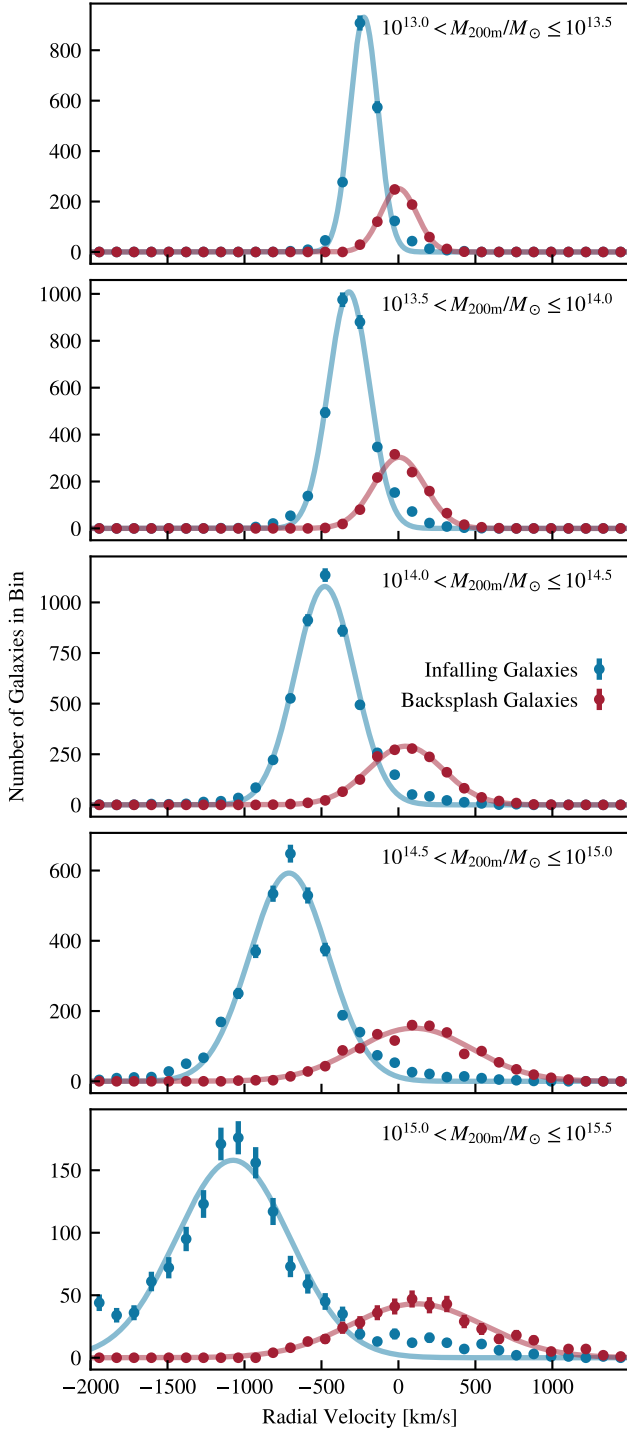


Figure 4. The radial velocity distributions for galaxies within $1 < R/R_{200,\text{mean}} < 2$, split by infalling/backsplash category (blue and red points, respectively), split by halo mass (different panels). Radial velocities are binned in 32 equally spaced linear bins between $-2000 \text{ km s}^{-1} \leq v_r \leq 1500 \text{ km s}^{-1}$. The background lines show gaussian fits to the binned data to guide the eye. Infalling galaxies have, almost universally, a negative radial velocity (as expected). Backsplash galaxies have a gaussian distribution of radial velocities centred around, approximately, zero; at higher masses, though, the backplash galaxies are biased to having a mean velocity greater than zero (i.e. there are more galaxies on their way back out of the cluster than falling back in). Notably the results remain qualitatively consistent (other than the relative abundances) when only considering galaxies within $R < 1.24R_{200,\text{mean}}$.

It is hence clear why it is common to use phase-space information to separate orbiting and infalling galaxies, as in [Farid et al. \(2022\)](#). It is possible to easily classify a galaxy into the infalling or backplash bins based upon the radial velocity alone. Unfortunately, measuring the radial velocity of galaxies relative to their cluster is extremely difficult in observations. Velocities measured in observations cannot decompose components into three dimensions. Only velocities along the line of sight can be measured, with redshift offsets, but these provide little information about the radial velocity of the galaxy (this is only one component of three). Thus, given a line of sight velocity of zero, it is unclear whether this is an infalling galaxy with a high v_r , just tangential to the viewer, or a backplash galaxy with $v_r = 0$ at apocentre.

As such, classifying a galaxy based upon its intrinsic properties (e.g. luminosity) so that it can be targeted for confirmatory follow-up and further study is desirable.

In Fig. 5 we show a number of galaxy scaling relations for the galaxies in our sample, split into three categories: backplash (red), infalling galaxies (blue), and for comparison purposes, all galaxies in the TNG300 simulation (dark blue and background contours). Each line shows the median relation for these galaxies, binned in 16 equally log-spaced bins across the mass range shown in the figure. In the background we show scatter plots, coloured appropriately, for both the backplash and infalling galaxies, to give some sense of scatter in the relations.

The general picture from these scaling relations is that backplash galaxies are redder and less gas-rich than their infalling counterparts. All scaling relations are shown against the final, $z = 0$, stellar mass of the galaxies (i.e. what would be observed), rather than the pre-infall mass of the galaxies. We choose to do this as we aim to classify galaxies based upon their properties, and pre-infall properties of galaxies cannot be observed. Generally, infalling galaxies are consistent with the entire TNG300 population.

In the top left panel we show the black hole mass, which is the sum of all black hole masses that are bound to the substructure. We see that, below $M_* \approx 2 \times 10^9 M_\odot$, backplash galaxies (as the median) have no black holes, but above $M_* \approx 10^{10} M_\odot$ backplash galaxies follow the same trend as infalling galaxies. We dedicate §6 to the investigation of this surprising property of backplash galaxies in TNG300.

The top centre panel shows the *i*-band (typically the brightest out of the eight bands in the TNG catalogue) magnitude of galaxies as a function of their stellar mass. Backsplash galaxies live in a very thin band around the median, with far (0.5dex) higher (dimmer) magnitudes than their infalling counterparts, up to $M_* \approx 10^{10.5} M_\odot$. This higher mass-to-light ratio for backplash galaxies suggests that their stars are redder and older, and has been observed in prior studies ([Knebe et al. 2011](#)). At $M_* > 10^{10.5} M_\odot$, AGN play an important role in shutting down star formation in the galaxies, quenching them internally (rather than through external processes such as ram-pressure stripping), reducing their mass-to-light ratio ([Donnari et al. 2019](#)).

The top right panel shows the half-mass stellar size of galaxies. We see that backplash galaxies are biased towards having higher sizes than their infalling counterparts at $M_* < 10^{10} M_\odot$, though there is a high degree of overlap in the two size distributions. We dedicate §5 to the investigation of size differences between backplash and infalling galaxies.

In the centre left panel we show the stellar mass ratio M_*/M_H , the fraction of bound mass to the galaxy that is in the stellar component. Backsplash galaxies and infalling galaxies show a similar stellar mass ratio across the mass range to their infalling counterparts,

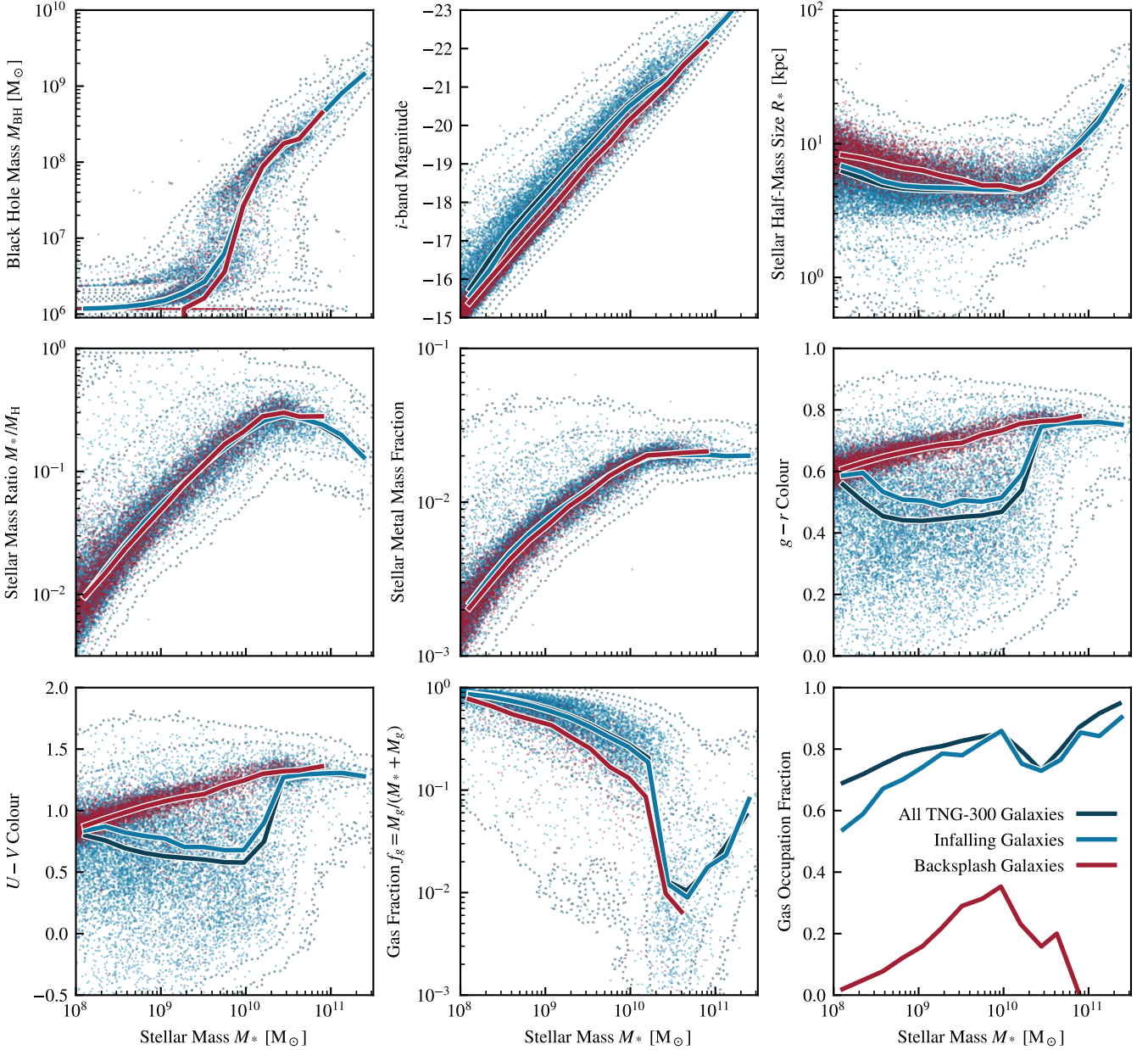


Figure 5. A collection of common galaxy scaling relations, split into three groups: backslash galaxies (red points and line), infalling galaxies (light blue points and line), and all TNG300 galaxies (dotted contours and dark blue line). Lines show the median binned in 16 equally log-spaced bins across the stellar mass range shown, and the points show all galaxies. All scaling relations are shown as a function of galaxy stellar mass, here defined to be the mass contained within twice the stellar half-mass radius. Here we see that backslash galaxies have lower mass black holes, high mass to light ratios, and are generally redder, larger, and have significantly lower gas occupation fractions than their infalling counterparts.

suggesting that backslash galaxies have not preferentially lost or gained stellar mass, and that differences in their stellar properties are due to rearrangement of stars and star formation either temporally (e.g. quenching) or spatially (e.g. tidal heating).

The centre panel shows the stellar metal mass fraction (frequently referred to in simulations as ‘metallicity’), which is the fraction of the stellar mass in the galaxy that is made up of elements other than hydrogen and helium. Below $M_* < 10^{10} M_\odot$ backslash galaxies have a slightly (0.05–0.1 dex) lower metallicity than infalling galaxies, and have far fewer high metallicity galaxies.

The $g - r$ and $U - V$ colours of the galaxies are shown in the centre right and lower left panels, confirming the suspicions from Fig. 1

that backslash galaxies are on average redder than infalling galaxies. The backslash galaxies live in the well-studied red sequence of quenched galaxies, indicating that they have been quenched for a long time (> 1 Gyr). Though there are many quenched infalling galaxies, there is a significant active population with colour $U - V \approx 0.5$. At the high mass end, $M_* > 2 \times 10^{10} M_\odot$, we again see that the infalling galaxies become quenched (coinciding with high black hole masses, and high mass-to-light ratios in the upper panels), further indicating that AGN feedback rapidly quenches galaxies at this mass.

In the final two (lower centre and right) panels, we consider the

gas fraction of the galaxies. The gas fraction,

$$f_g = \frac{M_g}{M_* + M_g}, \quad (2)$$

is shown for galaxies with at least one bound gas particle in the lower centre panel. Even in galaxies that retain gas, the gas fractions of backplash galaxies are significantly lower than their infalling counterparts. Another indicator of the significance of AGN feedback can be seen at $M_* \approx 2 \times 10^{10} M_\odot$, where all galaxies see a sharp downturn in gas fraction thanks to the evacuating effect of these objects.

In the bottom right panel we show the gas occupation fraction of galaxies as a function of their stellar mass. The gas occupation fraction is defined as the fraction of galaxies in a bin that have a gas mass greater than zero, i.e. they contain bound gas particles. Notably, backplash galaxies have significantly lower (3–4 times) gas occupation fractions than infalling galaxies. This staggering difference is even higher when considering clusters with $M_{200,\text{mean}} > 10^{14} M_\odot$, (not shown for brevity) where nearly all backsplashers have no gas. Such low gas occupation fractions likely originate from strong ram pressure stripping of galaxies as they pass through the cluster (Simpson et al. 2018).

4 IDENTIFYING CRITICAL PROPERTIES

In this section, we use a decision tree classifier to identify backplash galaxies based upon their intrinsic properties. We choose a decision tree classifier as it is highly interpretable; the outputs from the model are simply bisections in each parameter space, ranked by their importance. Through the decision tree, we can identify (in a relatively unbiased way) which features of galaxies can be used to classify them as backplash or infalling galaxies, before moving on to the physical interpretation of these features. We note that the main reason for employing the machine learning model in this context is not necessarily to enable the use of an off-the-shelf model for using intrinsic properties to identify backplash galaxies, as the specific normalisations of such quantities (stellar mass, black hole mass, galaxy colour, etc.) are usually not entirely converged within the simulation and modelling errors may lead to offsets to observational data (Schaye et al. 2015; Pillepich et al. 2018a). Instead, we wish to use the model to tell us which, out of all available properties, are those critical to bisecting the population of backsplashing and infalling galaxies.

4.1 Training the decision tree

Once we have identified all backplash galaxies and infalling galaxies within the radius range $1 < R/R_{200,\text{mean}} < 2$, we assign all galaxies integer labels (zero for infalling galaxies, and one for backplash galaxies). Alongside this, we collate all (reasonable) galaxy properties from the publicly available TNG SubFind catalogues. These are shown in Table 1, with the properties of their hosts that are also included in their description. Finally, we include the current distance between the galaxy and cluster centre, R_{gal} in units of the cluster $R_{200,\text{mean}}$. Most properties are logarithmically scaled (R_{gal} is not), as this eases in the interpretation of the results from a physical standpoint. As the decision tree framework does not accept any values that are infinity or not a number, we bound all scaled values as a lower limit of -10. Typically when a property has a physical value of zero (and hence logarithm of $-\text{inf}$), the decision tree uses a cut to check for occupation of this value (e.g. gas mass), so the specific value chosen here does not impact our results.

The results in this section are based upon the clusters with mass $10^{14} < M_{200,\text{mean}}/M_\odot < 10^{15}$, to reduce complexities associated with cluster evolution but to still leave a large sample of clusters (215) and backplash galaxies. Additionally, we make a cut in galaxy stellar mass $M_* > 10^8 M_\odot$ (10 particles), mainly to ensure that there are enough particles such that the occupation of the subhalo is accurate. At low masses, where there are only one or two particles in a subhalo, there may be many similar subhaloes that are unoccupied simply by chance, as star formation in the TNG model is a stochastic process (Genel et al. 2019; Keller et al. 2019).

To train the decision tree, we transform all associated features (N_{feat}) with the N_{gal} galaxies into a $N_{\text{feat}} \times N_{\text{gal}}$ matrix, with an associated one dimensional array containing the integer labels. These two arrays are then shuffled, to simplify training and validation splits.

We leverage the decision tree classifier object already implemented in the PYTHON package SCIKIT-LEARN (Pedregosa et al. 2011). When training, we use the Gini impurity for the split criterion, the “best” split strategy, a maximum tree depth of 6, and a minimal impurity decrease of 0.001. Choosing instead to use the entropy information gain criterion, or larger tree depths, do not qualitatively change our results. We choose the depth and minimum impurity decrease to make the tree easier to visually inspect, and for performance reasons.

To investigate the accuracy of our model, we use a 80–20 validation and training split. Our decision tree gets a 20% cross-validation score of 89%, meaning that when trained on a 80% of the data, and tested on 20%, we are able to correctly predict the classification of a galaxy 89% of the time. However, as we are mainly interested in the ability of the model to predict whether or not something is a backplasher, rather than the ability of the model to predict if a galaxy is infalling, we now focus on our positivity and false positive rate. When considering only galaxies that are backsplashes, we have a 20% positivity rate of 78%, meaning that we mis-classify 22% of backplash galaxies as infalling galaxies. However, we only have a 7% false-positive rate, meaning only 7% of the galaxies predicted by the model to be backplash galaxies are actually infalling. The accuracy of our decision tree model is comparable to other recent studies that additionally employ phase-space information, with Farid et al. (2022) able to achieve an 83% classification accuracy when using phase-space information and sSFR with a random forest model. The hard classification model² in Farid et al. (2022) is designed to separate infalling galaxies and those within the cluster, however, and does not explicitly classify backsplashes. Their hard classification model cannot accurately predict the existence of bound structures to the cluster in the range $R > R_{200,\text{mean}}$.

Such a high level of accuracy is surprising given the large level of overlap between the backplash and infalling population (see Fig. 5). For instance, making a cut based on simple population statistics, with $R/R_{200,\text{mean}} < 1.2$, and a red sequence cut in $g - r$ magnitude, returns a positivity rate of under 30% (though with only a 3% false-positive rate owing to the markedly lower number of galaxies classified as backsplashes).

Galaxy Property	Aperture	Log?
Total black hole mass	Total	✓
Total black hole mass accretion rate	Total	✓
Magnetic field strength in disk	Total	✓
Magnetic field strength in halo	Total	✓
Center of mass	Total	×
Gas metal mass fractions for each species	Twice half-mass radius, half-mass radius, max radius, SF gas only	✓
Gas total metallicity	Twice half-mass radius, half-mass radius, max radius, SF gas only	✓
Galaxy half-mass radius (per species)	Total	✓
Galaxy half-mass radius (total)	Total	✓
Number of particles (per species)	Total	✓
Number of particles (total)	Total	✓
Total mass	Total, half-mass radius (per species, total), twice half-mass radius, max radius	✓
Subhalo position in box	Total	✓
Subhalo instantaneous SFR	Total, twice half-mass radius, max radius	✓
Subhalo spin parameter κ	Total	✓
Star metal mass fractions for each species	Twice half-mass radius, half-mass radius, max radius	✓
Star total metallicity	Twice half-mass radius, half-mass radius, max radius, SF gas only	✓
Magnitude in U, B, V, K, g, r, i, z bands	Total	×
Total mass within K-band half-light radius	Total	✓
Half-light radius in K band	Total	✓
1D velocity dispersion of all member particles	Total	✓
Maximum value of the spherically-averaged rotation curve V_{\max}	Total	✓
Radius at which V_{\max} is achieved.	Total	✓
Total mass currently decoupled as winds	Total	✓
$U - V$ and $g - r$ colour	Total	×
Cluster Property	Aperture	Log?
Group centre of mass	Total	×
Group gas metal mass fractions for each species	Total	✓
Group gas metallicity	Total	✓
Group star metal mass fractions for each species	Total	✓
Group star metallicity	Total	✓
Group aperture masses	$R_{500,\text{crit}}, R_{500,\text{mean}}, R_{200,\text{crit}}, R_{200,\text{mean}}, R_{200,\text{tophat}}$	✓
Group aperture radii	$R_{500,\text{crit}}, R_{500,\text{mean}}, R_{200,\text{crit}}, R_{200,\text{mean}}, R_{200,\text{tophat}}$	✓

Table 1. *Top:* The galaxy properties used to train the decision tree. In the second column, the aperture within which this quantity is calculated is noted. Here, total refers to the total bound mass to this subhalo. In this column, half-mass radius refers to the *stellar* half-mass radius. *Bottom:* The cluster properties associated with each galaxy. These are the properties of the cluster that the galaxy has backsplashed from or is falling into. The final column for both shows whether or not the value is pre-scaled logarithmically before its use in the decision tree. Note that this does not affect results, as the decision tree simply performs a set of bisections, but it does aid in the inspection of the results.

4.2 Interpreting the model

That we can classify galaxies as backsplashers from their intrinsic properties without detailed kinematic information is interesting, but not as interesting as answering *why* we can classify them. Fig. 6 shows the feature (Gini) importances for the top ten features in the model for bisecting the infalling and backplash galaxy populations. Their correlations are also shown in Fig. 7, where backplash galaxies are shown in red, and infalling galaxies in blue. In this figure, dashed black lines show the bisections that the decision tree predicts are the most likely to segment the two populations, with the series of cuts in the tree shown for the leaf node with the highest number of backplash galaxies. The top right panels show the same projections but with the cuts applied to the whole population.

The most important feature in the entire model is $\log_{10} M_g$, the gas mass of the galaxy. We can see that this feature is used for occupation testing by the model, with the majority of backplash galaxies (see the bottom right panel of Fig. 5) containing zero gas. This is

even more stark when applied to the more massive clusters, with gas occupation fractions of backplash galaxies reducing as the clusters get more massive due to increased ram pressure stripping.

For the second most important feature, it is fair to say that the decision tree has ‘learned’ about the geometry of the problem (Fig. 3), with the likelihood of a galaxy being a backplasher dropping rapidly with distance from the cluster centre. The decision tree places a cut when just over 50% of the galaxies are likely to be infalling ($R_{\text{gal}}/R_{200,\text{mean}} = 1.41$). This is clear to see as well in Fig. 7, where the frequency of backplash galaxies clearly drops off with increasing R_{gal} .

Next, there are three measures of galaxy size. In decreasing order of importance, the model finds that $\log_{10} R_{1/2,\text{H}}$ (total bound half-mass radius), $\log_{10} R_{1/2,\text{DM}}$ (dark matter half-mass radius), and $\log_{10} R_{1/2,*}$ (stellar half-mass radius) are useful indicators of backplash status. As this topic is somewhat complex, we dedicate an entire section of the paper to it (§5), but briefly we see that backplash galaxies tend to have larger stellar half-mass sizes, and larger (or smaller) dark matter half-mass sizes for higher mass (lower mass), than their infalling counterparts.

The model finds that a cut in i -band magnitude is useful in segmenting the two populations, but it chooses a very low luminosity

² Note that ‘hard’ in this context implies that the model must make a choice to classify an object within a group, as opposed to ‘soft’ classification that assigns probabilities of belonging to a given group to each object.

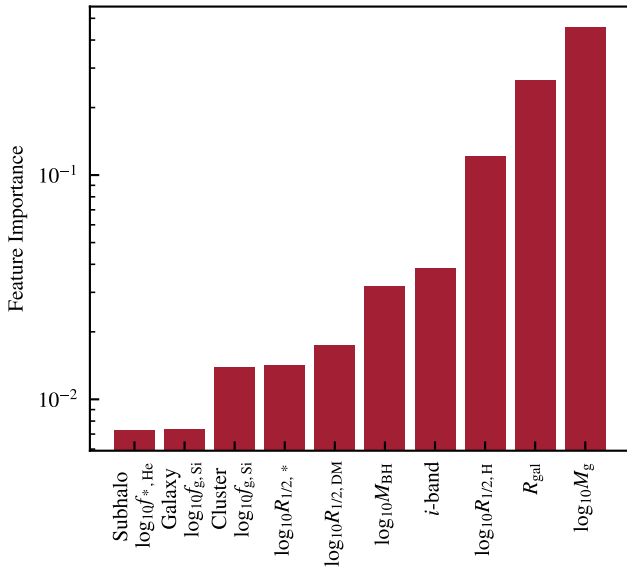


Figure 6. Gini importances of the top ten highest ranked features in the TNG300 datasets, when classifying backplash galaxies. A higher importance score corresponds to a higher level of information gain when bisecting this property. Descriptions of the symbols used here are available in the text.

cut (with $i < -16.7$). In Fig. 5, we see that at these low magnitudes the overlap between the infalling and backplash populations becomes higher, making segmenting them based upon this property troublesome. Although the prescence of this cut is useful, it is likely to be more numerically motivated, as at this luminosity (and hence mass) photometry is not particularly well resolved, with the star formation history of the galaxy being traced by around 10 stellar particles. With increasing resolution, the turn down of the $i/\log M_*$ relation seen in Fig. 5 at the lowest luminosities would likely disappear, but it is notable that the model picks up numerical differences between populations, as well as physical differences, indiscriminately.

In a similar fashion to the gas mass of galaxies, the model uses the black hole mass as an occupation check, with it placing a cut in the black hole mass $\log_{10} M_{\text{BH}}$ below the seed mass of black holes in the simulation. This is why in the top right of Fig. 7, the black hole mass panels contain zero points; the model has selected only galaxies that currently have zero black hole mass. As with the sizes, we dedicate a section (§6) to the investigation of this.

Finally, the model finds that some species fractions contribute to the ability to bisect the two populations. First, the cluster silicon gas fraction ($\log_{10} f_{g, \text{Si}}$), which is the mean silicon gas fraction within all gas particles bound to the cluster associated with the galaxies. Secondly, we find that, in galaxies that retain their gas, their gas silicon abundance is a useful criterion to bisect on. Finally, the fraction of galaxy stellar mass that is helium ($\log_{10} f_{*, \text{He}}$) contributes to the ability to bisect the two populations. [Vogelsberger et al. \(2018\)](#) and [Barnes et al. \(2018\)](#) investigated clusters in the TNG300 simulation, and showed that cool-core clusters, with relaxed morphologies, have significantly higher levels of enrichment in their cores. This may suggest that higher cluster enrichment levels may correlate with different tidal interactions between galaxies and the cluster, but we see no significant correlation between $\log_{10} R_{1/2, \text{DM}}$ and $\log_{10} f_{g, \text{Si}}$ in Fig. 7. It is additionally clear that further cuts on the cluster silicon abundance and galaxy helium abundance would be able to separate out a cleaner sample of backplash galaxies, but along with the low

importance indicated by the decision tree it is likely that this is simply by chance.

5 UNDERSTANDING GALAXY SIZES

In Fig. 6, we saw that some of the leading-order features separating backplash and infalling galaxies were their sizes in various mass types (total mass, dark matter mass, and stellar mass). These splits were used downstream of the occupation cut in gas mass, with star formation rates in the halo catalogues computed instantaneously from the bound gas (and hence all of the backplash galaxies were passive). This means that these features are useful irrespective of active/passive status of galaxies as seen by the model.

In Fig. 8 we show the relationship between total bound mass of galaxies and their stellar and dark matter half-mass sizes (top and bottom panels respectively). These relationships are split by their active and passive nature for infalling galaxies, with backplash galaxies grouped together (the quenched fraction of backplash galaxies is 94% so splitting these makes little sense). Here, we take the active/passive threshold to be a specific star formation rate $s\text{SFR} = \text{SFR}/M_* = 10^{-11} \text{ year}^{-1}$, computed from the instantaneous gas star formation rate. Only galaxies with at least $M_* > 10^8 M_\odot$ are included in this analysis, but all clusters are included.

As in [Genel et al. \(2018\)](#), we find that quenched galaxies have significantly larger stellar sizes than their active counterparts. At the lowest masses ($M_H < 10^{11} M_\odot$), backplash galaxies show even larger stellar sizes than their quenched counterparts.

In [Genel et al. \(2018\)](#) one of the main explanations for low-mass galaxies being large is that they have experienced significant tidal heating, as the sample of low mass galaxies are almost entirely satellites. Here, we are able to show that ‘field’ galaxies (in this context, these are galaxies that have not been processed by the cluster yet, so infalling galaxies) that are quenched have experienced similar size growth at low masses as the general quenched population, suggesting a different explanation is warranted.

At the high-mass end of the stellar sizes, we see that backplash galaxies grow their sizes faster (at lower masses) than infalling galaxies, but there are few backplash galaxies of this mass and as such this result is tenuous. At the highest masses, $M_H > 10^{12} M_\odot$, quenched and active galaxies have similar sizes when separated by instantaneous specific star formation rate. This similarity is likely due to the method of quenching; these galaxies are mainly quenched by their central AGN periodically, going through phases of feedback and gas evacuation, followed by fresh accretion and cooling leading to increases in star formation. Here the quenched and active separations only show different epochs of the evolution of these galaxies.

The dark matter sizes of galaxies are generally more similar, with a notable kink in the infalling galaxy sizes at $M_H = 10^{11} M_\odot$ that is not present in the backplash galaxies. This kink is likely caused by the introduction of black holes to the haloes, which occurs at total FoF halo masses of $7.4 \times 10^{10} M_\odot$ in the TNG model, with AGN feedback having been shown to decrease the central density of dark matter in simulations ([Duffy et al. 2010](#)).

At masses below the kink, backplash galaxies are the largest, but this trend is reversed after the kink where they are the smallest. This indicates that at low masses, similar processes are governing the size differences (i.e. low mass galaxies have large stellar and dark matter sizes for the same reason) but at higher masses the stellar component and dark matter components are affected by different processes. In addition, at masses below $M_H < 10^{11} M_\odot$, stellar and dark matter half-mass sizes are comparable, of order 10 kpc. At higher masses,

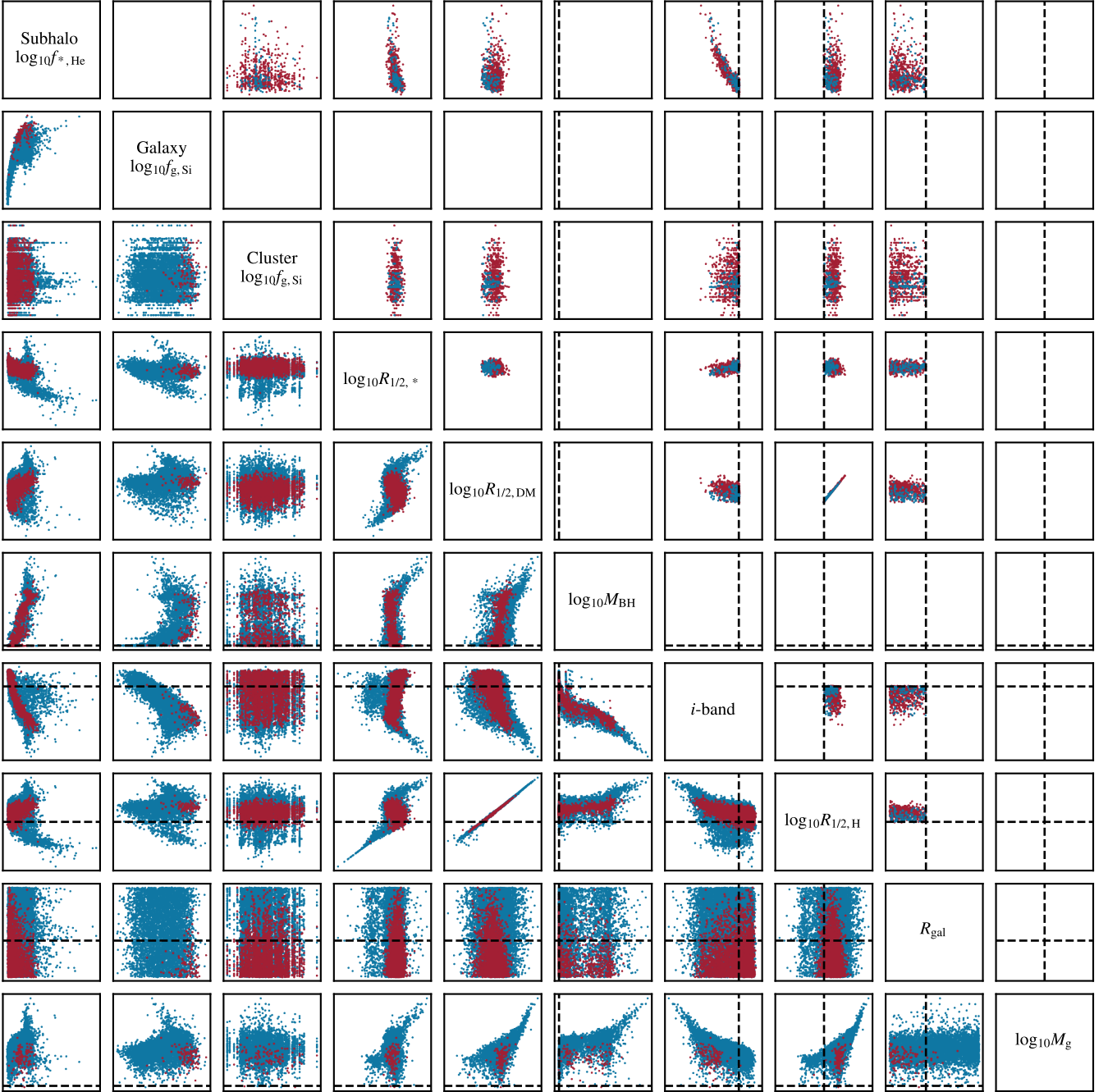


Figure 7. The highest ranked features from Fig. 6 scattered against each other. The bottom left triangle shows all galaxies in the sample, with blue points representing infalling galaxies and red points representing backslash galaxies. The dashed lines show the cuts identified by the decision tree based on the top five most important features, with the top right panels showing the resulting parameter space after the cuts have been applied to find the largest contiguous volume of backslash galaxies. This time, the blue points are plotted on top of the red points to highlight false positive detections. In this region, we find 603 backslash galaxies with a false-positive rate of 15%.

the dark matter half-mass size is significantly larger, breaking the scales between the dark matter and stellar components.

In Fig. 9 we show the two measures of galaxy size against each other, alongside the softening scale. Campbell et al. (2017) found that galaxy stellar sizes flatten at a characteristic scale (2.8 times the softening length $\epsilon_{DM,*}$, which for TNG300 is 1.48 kpc at redshift $z = 0$), and this appears to be true within TNG300, also. However, whilst the active galaxy sizes saturate at around 4.2 kpc, as predicted by Campbell et al. (2017), our quenched galaxy sizes (and backslash

sizes) rise above this level for the lowest masses. As TNG300 haloes and galaxies grow, they begin to revert to the 1:1 relation (at dark matter sizes above 100 kpc).

Ludlow et al. (2019a), Ludlow et al. (2019b), and Ludlow et al. (2020) discuss origins of this potentially spurious size growth in galaxies, and suggest that its origins lie in 2-body scattering between different particle species (in this case, dark matter and stars) with different masses. In this scenario, energy is transferred from the more massive component (dark matter) to the less massive com-

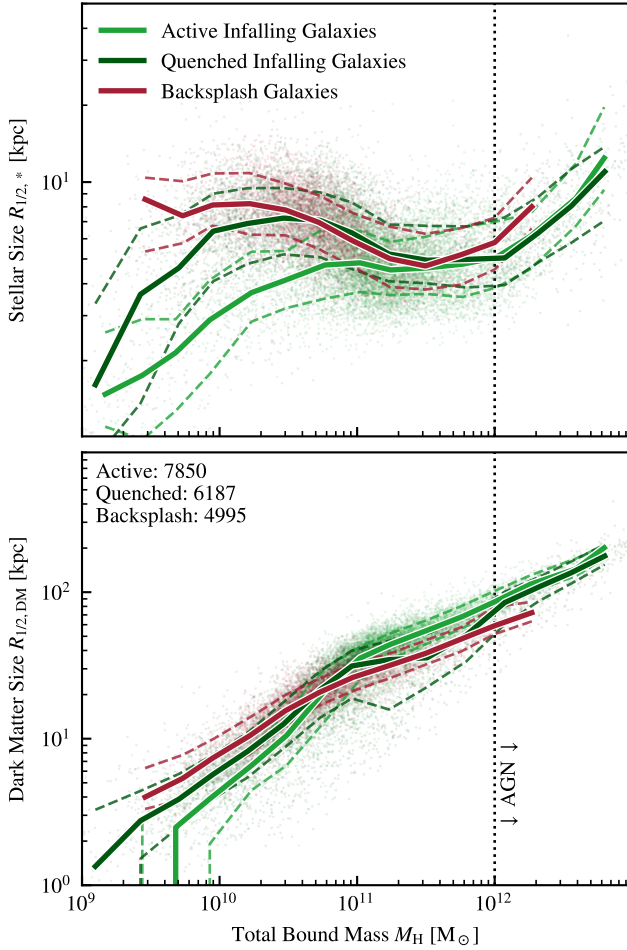


Figure 8. Mass-size relations for backplash galaxies (red) and infalling galaxies split into quenched (dark green) and active (light green) populations by specific star formation rate $sSFR = 10^{-11} \text{ year}^{-1}$. In the background the scatter shows all galaxies in the sample, with the solid lines representing the median in 16 equally log-spaced bins, and dashed lines showing the 16–84 percentile range. The top panel shows the stellar half-mass radius, and the bottom panel shows the dark matter half-mass radius. The dotted vertical line shows the total bound mass at which AGN feedback becomes significant, leading to a noticeable up-tick in the stellar sizes. The numbers in the top left of the bottom panel show how many galaxies are in each cut below the point at which AGN feedback becomes significant.

ponent (stars), causing the dark matter to be centrally concentrated within the halo and the stellar component to be dynamically spread. Galaxies that are artificially inflated by 2-body scattering are then expected to have more massive, cuspy, inner dark matter profiles, and hence smaller dark matter sizes at a given mass.

Our relationship between $R_{1/2,DM}$ and $R_{1/2,*}$ is generally flat at dark matter sizes below 100 kpc (i.e. it does not continue down the 1:1 relation), indicating that sizes are propped up in this case by softening inflation, with a minimal stellar (and dark matter) size set by $2.8\epsilon \approx 4.5 \text{ kpc}$. There is clearly more to this, however, with there being significant differences between active and passive infalling galaxies, as well as the backplash population.

In TNG-50, where significantly higher resolution simulations are available (a rough factor of 100 smaller particle masses), [Pillepich et al. \(2019\)](#) showed that at the resolution of TNG300, (roughly TNG-50-3) the stellar half-mass sizes of galaxies were not con-

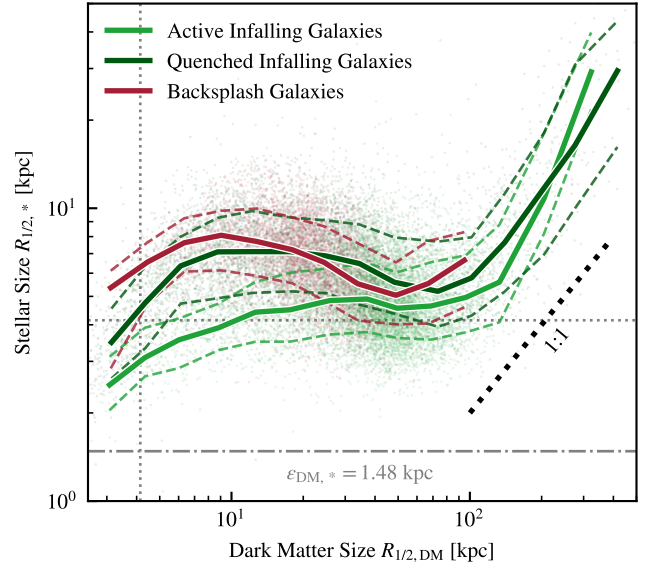


Figure 9. The two galaxy size measures from Fig. 8 shown against each other, with the same line styles and colours. In the background we show the 1:1 relation as a thick dotted black line, and for comparison purposes show the physical softening length at $z = 0$ in the TNG300 simulation of 1.48 kpc as a dot-dash grey line. We show, similarly to [Genel et al. \(2018\)](#), that quenched galaxies show larger stellar sizes on average even for a fixed halo size. The thin background dotted grey lines show the scale of 2.8ϵ , the characteristic scale identified in [Campbell et al. \(2017\)](#) at which sizes begin to flatten.

verged below $M_* < 10^{9.5} M_\odot$. Higher resolution generally gives smaller stellar sizes, consistent with the indications of [Ludlow et al. \(2021\)](#) that this may be due to lower levels of dynamical heating due to the lower dark matter masses used, or that the sizes are inflated due to oversoftening (as the chosen softening frequently scales with resolution). It is hence likely that 2-body scattering, as well as size inflation caused by softening, cause a systematic trend in our galaxy sizes at low masses ($M_* < 10^{9.5} M_\odot$) to become larger, meaning that the absolute sizes of our low-mass galaxies are overestimated. This does not mean, however, that any differences between the galaxy populations on these scales are entirely numerically driven. In particular, that we see differences in dark matter sizes at $M_H < 10^{11} M_\odot$ is reliable, as these sizes are both much larger than the softening scale (see Fig. 9) and generally would be made smaller, not larger, by 2-body scattering.

In Fig. 10 we show the mean-stacked stellar mass and dark matter mass profiles for the inner 20 kpc of all galaxies within each mass range. These profiles include all bound matter, and are stacked for three different mass ranges: $10^8 < M_*/M_\odot \leq 10^9$, $10^9 < M_*/M_\odot \leq 10^{10}$, and galaxies above $M_* > 10^{10} M_\odot$. The lines show the mean density, stacked across all galaxies in the mass range, with the final calculated mean the median of 1024 bootstraps (with replacement) of the original selection. The bootstrapping is used to estimate the error on the mean density, with the 16–84 percentile range shown as dashed lines. We also show the dark matter profiles of the same galaxies, stacked in the same way, as lighter lines in the background.

Fig. 10 shows that backplash galaxies have a significantly lower central stellar density than their infalling counterparts of the same mass. They also show a much more centrally concentrated density profile, in contrast to the quenched infalling galaxies which have a strong cusp in the central stellar density. These differences in stellar

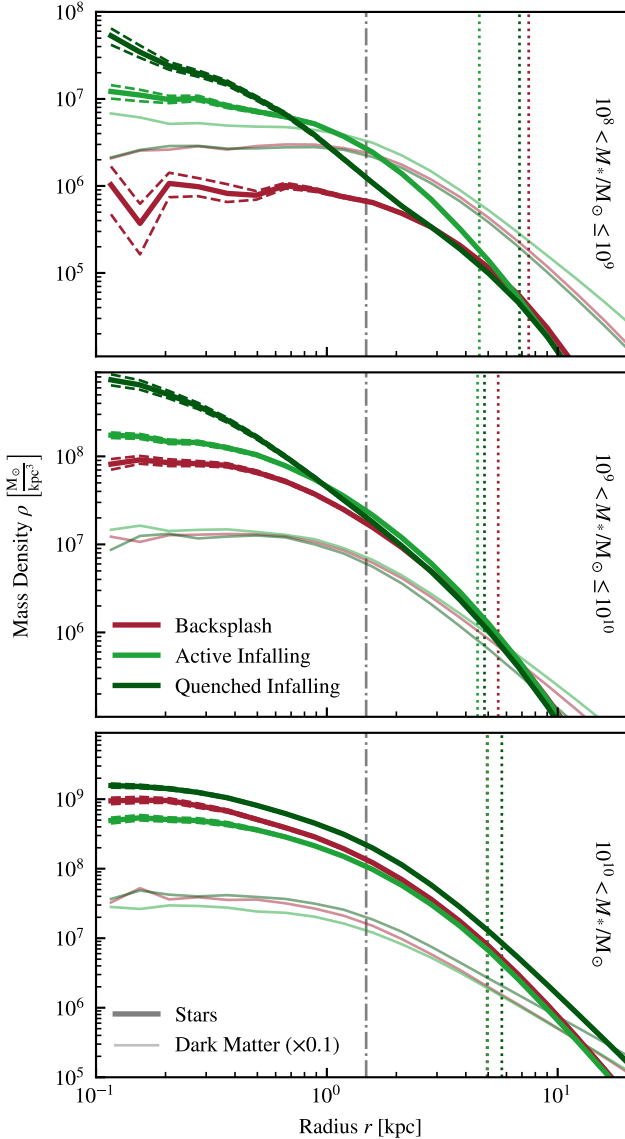


Figure 10. Mean stellar density profiles, split by final stellar mass (panels). Solid lines show the median, with the dashed lines showing the 16–84 percentile range, of 1024 mean-stacked bootstraps (with replacement) of all individual profiles. The vertical grey dot-dash line shows the gravitational softening used for stellar and dark matter particles, and the dotted lines show the median stellar half-mass radius for galaxies in each mass bin of the corresponding colour. In the background the lighter, thinner, line show the dark matter density profile, multiplied by 0.1 for clarity.

profiles are despite the dark matter profiles of the two classes of galaxies being extremely similar.

As in each cut the masses of the galaxies are constrained to be similar, we can see that although the sizes of the quenched infalling galaxies and backplash galaxies are similar, these originate through very different distributions. The quenched galaxies have a much steeper profile that drops off rapidly, whereas the backplash galaxies have a shallower profile that catches up and overtakes the quenched profile at large radii.

The flat central profiles of the backplash galaxies are consistent with those seen in Carleton et al. (2019), where the central stellar core is tidally heated through close interactions with the cluster halo as the galaxies orbit. Tidal heating injects energy into particles

within the galaxy as it falls into a cluster on a (crucially) eccentric orbit, with the shear forces on the bound particles changing rapidly with time. Tidal heating of backplash galaxies is further consistent with the increased sphericity seen in the shapes of backplash galaxies in prior works (Knebe et al. 2020).

Such tidal interactions have been suggested to be the origins of ultra-diffuse galaxies. A number of authors (e.g. Benavides et al. 2021; Trujillo 2021) have recently suggested that tidal heating and stripping processes could play a role in forming such UDGs. The suppression of the central stellar density of the backplash galaxies identified in this study certainly make them UDG candidates, and further suggest that a large number of UDGs near clusters may well be backplash galaxies. We caution, however, that the suppression of the central stellar density occurs close to the softening scale of the TNG300 simulation, making the close gravitational interactions less accurate than would be ideal for studying such complex dynamics. These results suggest that follow-up studies should focus on these low-mass backplash galaxies, as they are potentially the most distinct from their infalling counterparts, but due to the limited resolution of TNG300 we are unable to make direct comparisons to nature.

In Fig. 11 we show the outer (total mass, though in this region the mass density is dominated entirely by dark matter) profiles of our haloes. Here, we split by halo mass, but only include galaxies that are occupied by at least $M_* > 10^8 M_\odot$ for consistency. We see that at masses $M_H > 10^{10} M_\odot$ there is significant disruption of the backplash subhaloes, leading to smaller dark matter half-mass sizes (as can be seen in Fig. 10, the inner dark matter profiles are consistent for backplash and infalling galaxies). This suggests that there has been significant tidal stripping of subhaloes as they have passed through the cluster, with the strength of the stripping increasing with increasing subhalo mass. This is consistent with the results from Jiang & van den Bosch (2016) who studied the disruption of subhaloes in the Bolshoi simulation, and found that the tidal mass loss rate, $dM_H/dt \propto M_H^{1.07}$, shows superlinear growth with subhalo mass.

van den Bosch (2017), van den Bosch et al. (2018), and van den Bosch & Ogiya (2018) all discuss the potential origins of forces leading to tidal stripping, and whether the disruption of substructure is numerical or physical in nature. Notably, they find that disruption of subhaloes is converged over many softening scales and resolutions on short timescales (comparable to one or two cluster crossing times, see Fig. 10 in van den Bosch & Ogiya (2018)), but subhaloes continue to lose mass due to numerical effects on long timescales. van den Bosch & Ogiya (2018) focused only on subhaloes on small ($R/R_{\text{vir}} \approx 0.15$) circular orbits, however, meaning that in realistic scenarios (like our backplash subhaloes), the weaker tidal fields may have a less significant effect. As our backplash galaxies are typically on their way to their first periaapsis (i.e. they have only been influenced by the cluster for a relatively short amount of time), we suggest that the tidal disruption that our subhaloes have experienced is likely to be physical at large radii.

In summary, we have found that the stellar sizes of backplash galaxies are larger than the general field population, especially at low masses, whilst the bound mass (or dark matter mass) sizes of these galaxies are smaller than the field population, for a given subhalo or stellar mass. We have discussed how these differing sizes are likely due to tidal interactions with the host cluster: as galaxies fall in to the cluster, their cores ($r < 5$ kpc) are tidally heated (leading to a flatter inner stellar density profile, and larger stellar size, see Fig. 10), whilst their extremities ($r > 100$ kpc) are tidally stripped (see Fig. 11). This leaves us with galaxies that are dark matter dense, but

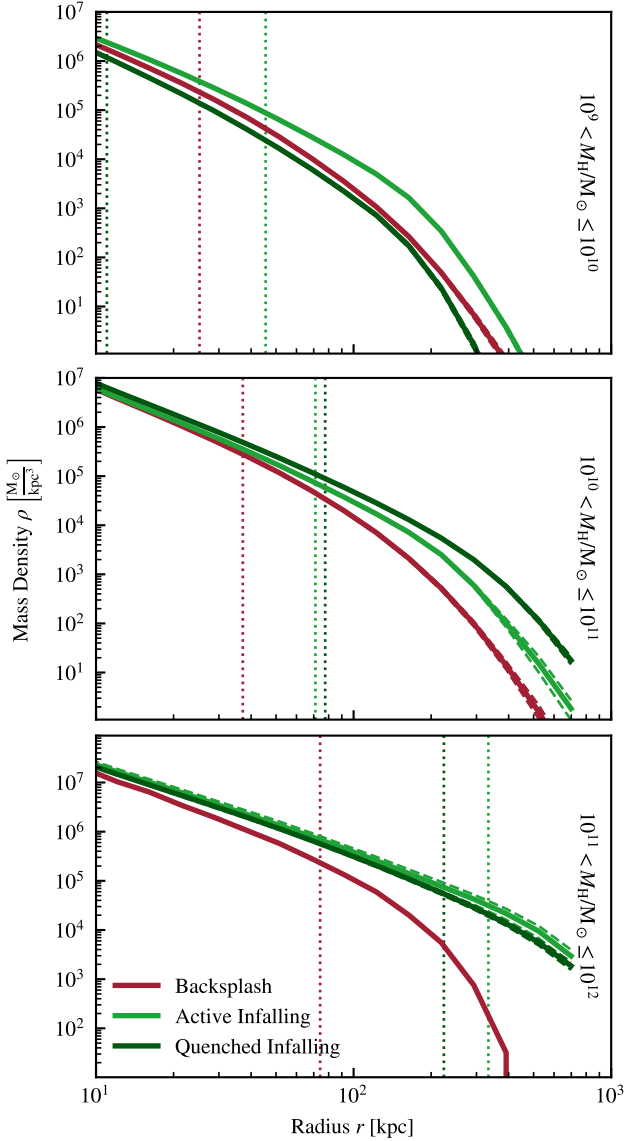


Figure 11. Mean total density profiles, split by final bound mass (M_H ; panels). Solid lines show the median, with the dashed lines showing the 16–84 percentile range, of 1024 mean-stacked bootstraps (with replacement) of all individual profiles. The dotted lines show the median bound mass half-mass radius for galaxies in each mass bin of the corresponding colour. Note that the horizontal range is shifted significantly from the same figure for the stellar component (Fig. 10). The inner regions are not shown as the profiles of all cuts are all consistent in dark matter and deviations are powered by differences in the stellar component.

gas and star poor, making the backslashing of galaxies a potential UDG formation mechanism, as suggested by prior authors.

6 BLACK HOLE OCCUPATION

To better understand both the radial profile differences explored in §5, and the importance of the black hole mass in classifying back-splash galaxies, we now consider the evolution of individual back-splash galaxies.

In Fig. 12 we show the properties of backslash galaxies falling into the most massive cluster in the volume ($M_{200,\text{mean}} = 2.13 \times 10^{15} M_\odot$)

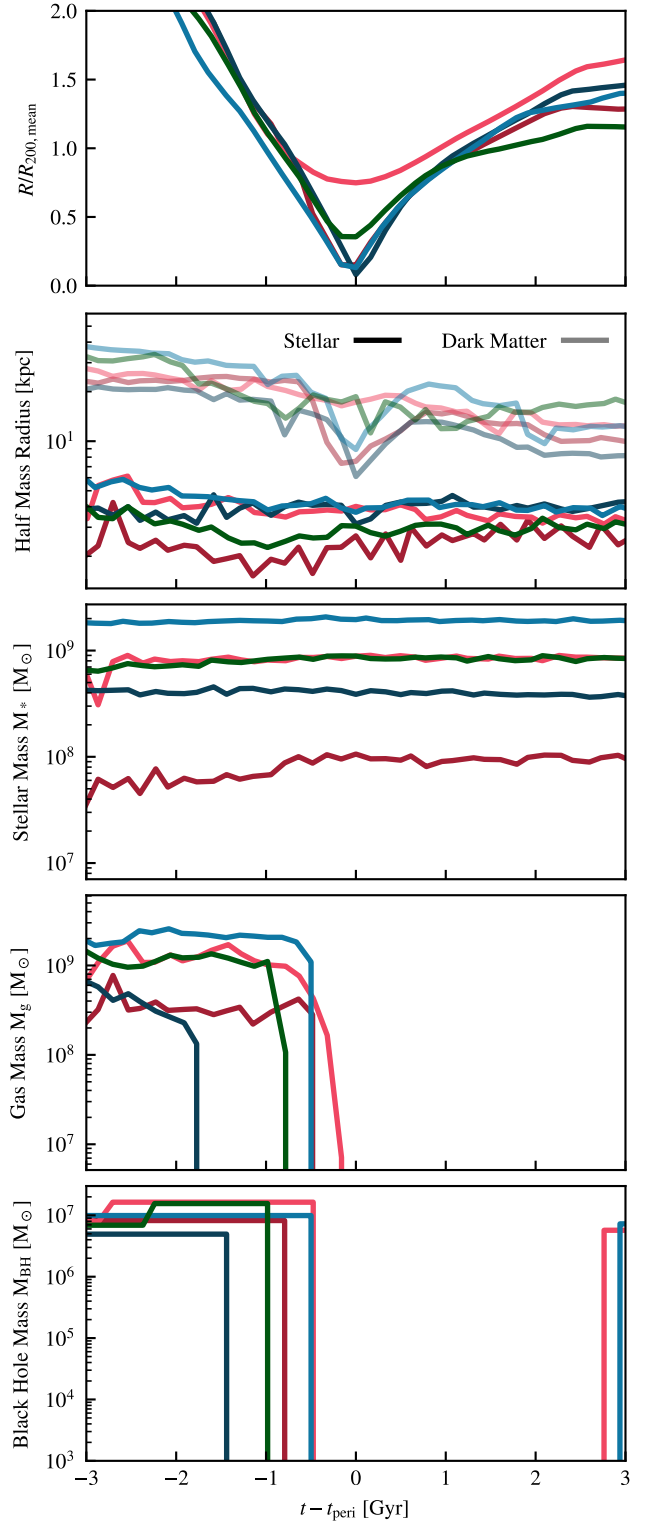


Figure 12. Tracks of cluster galaxies, rescaled to ensure that their pericentres overlap in time, all falling into the same ($M_{200,\text{mean}} = 2.13 \times 10^{15} M_\odot$ cluster). Each line (different colours) shows a different infalling galaxy). From top to bottom, the panels show the orbital radius of the galaxies, their stellar and dark matter half-mass radii, their bound stellar mass within twice the (stellar) half-mass radius, their bound gas mass (note when lines leave the bottom of the plot they have a value of zero) in the same aperture, and the total bound black hole mass, as a function of time.

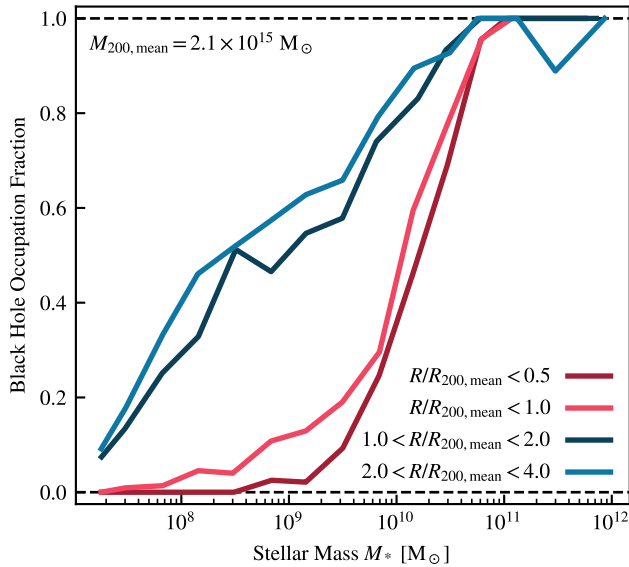


Figure 14. Shows the occupation fraction of black holes, computed as the number of galaxies in this bin that have a black hole divided by the total number of galaxies, for 16 equally log-spaced bins between the figure limits. Each line shows a different aperture around the cluster within which the occupation fraction is computed. The occupation fractions here are shown for the most massive cluster in the volume, and the same cluster shown in Fig. 12, with $M_{200,\text{mean}} = 2.13 \times 10^{15} M_{\odot}$, though these trends occur across the mass range.

for cluster galaxies (see their Appendix A). Notably, the model discussed in Bahé et al. (2021) also repositions only on gas particles, as typically the neighbour-finding structures (e.g. trees) within N-body codes are only set up to include gas particles for optimisation reasons. Our results, along with those in Bahé et al. (2021), suggest that the black hole occupation fraction of cluster galaxies is severely underestimated within cosmological simulations that employ such repositioning schemes.

Such issues with the repositioning of black holes are likely to persist amongst many of the state-of-the-art large-volume simulations, including the entire Illustris and IllustrisTNG suite, as well as the EAGLE suite and derivatives (Vogelsberger et al. 2014a; Schaye et al. 2015). Simulations that do not employ repositioning, such as the Horizon-AGN suite (Dubois et al. 2012), or Romulus (Tremmel et al. 2017), will not suffer from this artificial stripping of black holes from cluster galaxies. Prior work from Ragone-Figueroa et al. (2013) employed repositioning on all particle types, though unlike TNG has black hole growth dominated by accretion at all masses (Bassini et al. 2019), with TNG black holes showing merger-dominated growth at $M_{\text{BH}} > 10^8 M_{\odot}$ (Weinberger et al. 2018). It is possible that these authors, like the EAGLE simulations, included a maximal velocity difference between the black hole and repositioning candidates, but a full investigation of the implementation of black hole recentring strategies is out of the scope of this work. Additionally, modifying the neighbour finding structures used for repositioning to employ stellar particles for recentring purposes would insulate such schemes from these effects. The SIMBA simulation suite, that employs a loop over nearby stellar particles to compute accretion rates, already uses a recentring prescription that includes the use of stellar particles, and likely does not suffer from these black hole stripping issues (Anglés-Alcázar et al. 2017).

Haidar et al. (2022) investigated the occupation fraction of black

holes in a number of cosmological simulations, and found that the SIMBA suite, that repositions on stars as well as gas particles, have occupation fractions of close to 100% even down to low masses. They find that EAGLE and IllustrisTNG actually reduce their global occupation fractions of low-mass galaxies over time, due to the increasing fraction of galaxies resident in clusters. We have now demonstrated the specific numerical pathway through which these galaxies are stripped of their black holes.

There are a number of potential pitfalls for galaxy formation simulations with black hole stripping. Primarily, aside from the black hole occupation fractions being clearly incorrect (the artificial seeding procedure makes these numbers uncertain anyway), the contribution to the cluster energy budget from the AGN resident in cluster galaxies will be underestimated. Additionally, the merger rates of black holes, particularly those in the centres of clusters, will be overestimated, as will their masses. The impacts of these outcomes are not yet known, but as black hole seeding and AGN models are explicitly calibrated against observational data (e.g. Crain et al. 2015; Pillepich et al. 2018a) and as such these potential pitfalls may already be calibrated into the choice of free parameters.

7 CONCLUSIONS

Backsplash galaxies are galaxies that have previously had a pericentre within the bounds of a galaxy cluster, but have since migrated outside of most typical definitions of the cluster boundary. Their intrinsic properties are not well understood, as simulating such galaxies is numerically challenging due to the high inherent dynamic range of masses and spatial scales present in galaxy clusters.

In this paper we have explored the properties of backplash galaxies in the TNG300 simulation by tracing the orbits of galaxies with stellar mass $M_* > 10^8 M_{\odot}$ within $1 < R/R_{200,\text{mean}} < 10$ of our 1302 isolated clusters with $M_{200,\text{mean}} > 10^{13} M_{\odot}$. By classifying galaxies into ‘backplash’ and ‘infalling’ categories based upon whether the galaxy has previously been within $R_{200,\text{mean}}$ of the cluster re, we were able to find that:

- The abundance of backplash galaxies grows roughly linearly as a function of galaxy cluster mass, with $M_{200,\text{mean}} \approx 10^{14} M_{\odot}$ clusters on average hosting around 5 backplashers, and clusters with $M_{200,\text{mean}} \approx 10^{15} M_{\odot}$ hosting around 50 on average. Backsplash galaxies are significantly more common (relative to infalling galaxies) at smaller radii, with equipartition reached between the two populations at $R = 1.24 R_{200,\text{mean}}$. These two results suggest that observations targeting backplash galaxies should focus on the intermediate regions ($1 < R/R_{200,\text{mean}} < 1.5$) of the highest mass clusters $M_{200,\text{mean}} > 10^{14.5} M_{\odot}$, to reduce contamination and ensure adequate sampling.
- We verify that backplash galaxies and infalling galaxies are kinematically separated, with the separation increasing as a function of host cluster mass. Both backplash and infalling galaxies have a roughly gaussian radial velocity (v_r) distribution, with infalling galaxies having a mean velocity $\bar{v}_r < 0$ dependent on cluster mass ($\bar{v}_r = -1100 \text{ km s}^{-1}$ for $M_{200,\text{mean}} \approx 10^{15} M_{\odot}$). Backsplash galaxies have a typical mean radial velocity of $\bar{v}_r \approx 0$, with the width of the distribution dependent on cluster mass. These findings confirm that the use of phase-space information is an excellent way to classify backplash galaxies, if it is available (e.g. as in Farid et al. 2022).
- By considering typical galaxy scaling relations, we have shown that backplash galaxies in TNG300 are typically black hole-poor, have higher mass-to-light ratios, larger stellar sizes, redder colours,

and lower gas fractions than their infalling counterparts of a similar stellar mass. These characteristics are generally consistent with galaxies that have been ram pressure stripped, quenched, and tidally heated, processes thought to be common in galaxy clusters, and that have previously been shown to impact the evolution of backplash galaxies (e.g. [Simpson et al. 2018](#)).

- To investigate which intrinsic properties of galaxies (without considering phase-space information) are key to separating the infalling and backsplashing population we trained a decision tree classifier on all available (reasonable) properties from the TNG SubFind catalogues of our two populations. The classifier identified the most important features in separating the two populations of galaxies as the galaxy gas mass, distance from the cluster re, galaxy and halo size, magnitude, and black hole mass. Our decision tree classifier was able to classify backplash and infall galaxies with high accuracy, returning a 20% cross-validation score of 89%. When considering backplash galaxies alone, the classifier had a low (7%) false-positive rate, and a relatively low false-negative rate (22%). These levels of accuracy are comparable with other hard classifiers that do employ phase-space information, such as those used recently by [Farid et al. \(2022\)](#). Despite the high accuracy of the classifier, however, it would be impractical to use for observations, and as such we simply use the decision tree as a way to reduce the extreme dimensionality of our feature space, finding interesting galaxy properties to focus follow-up analysis on.

- Through the analysis of galaxy sizes and profiles, motivated by the decision tree, we showed that backplash galaxies have typically larger stellar sizes at low mass, and smaller dark matter sizes at high mass, than their infalling counterparts, even when accounting for the size growth of quenched galaxies due to numerical effects ([Genel et al. 2018](#)). We discussed how, despite numerical concerns with (relatively) low resolution simulations like TNG300, our results still suggest that the central regions of backplash galaxies are tidally heated, leading to flatter stellar inner density profiles. They also suggest that backplash galaxies are subject to tidal stripping, with the outskirts of backplash galaxies relatively devoid of dark matter relative to their infalling counterparts. We discussed how these processes contribute to the potential formation of UDGs near clusters, where UDGs are likely to be backplash galaxies.

- We investigated the low black hole occupation fraction of backplash galaxies by tracking the detailed properties of individual galaxies back over time. We showed that backplash galaxies typically lose all of their gas mass before reaching the pericentre of their orbit around the cluster, even when their orbit is shallow. We also showed how the black hole repositioning (or re-reing) prescription, which moves black hole particles within galaxies based on the local potential sampled by gas particles, leads to the extraction of black holes from infalling galaxies as they near the pericentre of their orbit. Such repositioning schemes, required to insulate black holes from spurious heating out of central galaxies and to maintain the efficiency of AGN feedback, hence come at the cost of underestimating the occupation fraction of black holes in cluster galaxies and hence their feedback contribution within clusters.

The large sample size of isolated massive haloes ($M_{200,\text{mean}} > 10^{13} M_{\odot}$) in TNG300 has enabled us to study a representative sample (over 5000) of backplash galaxies. We have found that the properties of these galaxies are crucially dependent on interactions with the host cluster that are still not well understood (or well modelled) in simulations, namely: tidal heating, tidal stripping, and ram pressure stripping. Thus, we find that, in general, backplash galaxies are an excellent marker in the sand for comparison to obser-

vations. In future work, higher resolutions and ever larger sample sizes, along with expanded observational samples from the upcoming DESI, Nancy Grace Roman Space Telescope, and Vera C. Rubin Observatory will provide a fruitful ground for exploration of galaxy formation models through the study of backplashers.

ACKNOWLEDGEMENTS

The authors thank Aaron Ludlow for conversations that significantly improved the discussion on galaxy sizes. The authors thank Yannick Bahé, Rüdiger Pakmor, Romeel Davé, and Rahul Kannan for conversations that significantly improved the discussion black hole loss for cluster galaxies.

Some of the computations in this paper were run on the FASRC Cannon cluster supported by the FAS Division of Science Research Computing Group at Harvard University. Some of the computations were performed on the Engaging cluster supported by the Massachusetts Institute of Technology. MV acknowledges support through NASA ATP 19-ATP19-0019, 19-ATP19-0020, 19-ATP19-0167, and NSF grants AST-1814053, AST-1814259, AST-1909831, AST-2007355 and AST-2107724. AS acknowledges support for Program number *HST*-HF2-51421.001-A provided by NASA through a grant from the Space Telescope Science Institute, which is operated by the Association of Universities for Research in Astronomy, incorporated, under NASA contract NAS5-26555.

Software citations:

- AREPO: [Springel \(2011\)](#); [Weinberger et al. \(2020\)](#)
- PYTHON: [Van Rossum & Drake Jr \(1995\)](#)
- MATPLOTLIB: [Hunter \(2007\)](#)
- SCIPY: [Virtanen et al. \(2020\)](#)
- SCIKIT-LEARN: [Pedregosa et al. \(2011\)](#)
- NUMPY: [Harris et al. \(2020\)](#)
- SWIFTSIMIO: [Borrow & Borisov \(2020\)](#); [Borrow & Kelly \(2021\)](#)

DATA AVAILABILITY

The data underlying this article are available in Zenodo at <https://dx.doi.org/10.5281/zenodo.6564713>. All data in this article were reduced from the publicly available TNG300-1 simulation data available at <https://tng-project.org> ([Nelson et al. 2019](#)).

REFERENCES

- Anglés-Alcázar D., Davé R., Faucher-Giguère C.-A., Özel F., Hopkins P. F., 2017, *MNRAS*, **464**, 2840
- Bahé Y. M., McCarthy I. G., Balogh M. L., Font A. S., 2013, *MNRAS*, **430**, 3017
- Bahé Y. M., et al., 2021, arXiv e-prints, p. [arXiv:2109.01489](#)
- Bakels L., Ludlow A. D., Power C., 2021, *MNRAS*, **501**, 5948
- Balogh M. L., Navarro J. F., Morris S. L., 2000, *ApJ*, **540**, 113
- Barnes D. J., et al., 2017, *MNRAS*, **471**, 1088
- Barnes D. J., et al., 2018, *MNRAS*, **481**, 1809
- Bassini L., et al., 2019, *A&A*, **630**, A144
- Bassini L., et al., 2020, *A&A*, **642**, A37
- Benavides J. A., et al., 2021, *Nature Astronomy*, **5**, 1255
- Borrow J., Borisov A., 2020, *The Journal of Open Source Software*, **5**, 2430
- Borrow J., Kelly A. J., 2021, arXiv e-prints, p. [arXiv:2106.05281](#)
- Campbell D. J. R., et al., 2017, *MNRAS*, **469**, 2335
- Carleton T., Errani R., Cooper M., Kaplinghat M., Peñarrubia J., Guo Y., 2019, *MNRAS*, **485**, 382

Crain R. A., et al., 2015, *MNRAS*, **450**, 1937

Dolag K., Borgani S., Murante G., Springel V., 2009, *MNRAS*, **399**, 497

Donnari M., et al., 2019, *MNRAS*, **485**, 4817

Dubois Y., Devriendt J., Slyz A., Teyssier R., 2012, *MNRAS*, **420**, 2662

Duffy A. R., Schaye J., Kay S. T., Dalla Vecchia C., Battye R. A., Booth C. M., 2010, *MNRAS*, **405**, 2161

Farid D., Aung H., Nagai D., Farahi A., Rozo E., 2022, arXiv e-prints, p. [arXiv:2205.01700](https://arxiv.org/abs/2205.01700)

Genel S., et al., 2018, *MNRAS*, **474**, 3976

Genel S., et al., 2019, *ApJ*, **871**, 21

Gill S. P. D., Knebe A., Gibson B. K., 2005, *MNRAS*, **356**, 1327

Haggar R., Gray M. E., Pearce F. R., Knebe A., Cui W., Mostoghiu R., Yepes G., 2020, *MNRAS*, **492**, 6074

Haidar H., et al., 2022, arXiv e-prints, p. [arXiv:2201.09888](https://arxiv.org/abs/2201.09888)

Hansen S. M., Sheldon E. S., Wechsler R. H., Koester B. P., 2009, *ApJ*, **699**, 1333

Harris C. R., et al., 2020, *Nature*, **585**, 357

Hunter J. D., 2007, *Computing in Science and Engineering*, **9**, 90

Jiang F., van den Bosch F. C., 2016, *MNRAS*, **458**, 2848

Jones M. G., Bennet P., Mutlu-Pakdil B., Sand D. J., Spekkens K., Crnojević D., Karunakaran A., Zaritsky D., 2021, *ApJ*, **919**, 72

Keller B. W., Wadsley J. W., Wang L., Kruijssen J. M. D., 2019, *MNRAS*, **482**, 2244

Kilborn V. A., Koribalski B. S., Forbes D. A., Barnes D. G., Musgrave R. C., 2005, *MNRAS*, **356**, 77

Knebe A., Libeskind N. I., Knollmann S. R., Martinez-Vaquero L. A., Yepes G., Gottlöber S., Hoffman Y., 2011, *MNRAS*, **412**, 529

Knebe A., et al., 2020, *MNRAS*, **495**, 3002

Koda J., Yagi M., Yamanoi H., Komiyama Y., 2015, *ApJ*, **807**, L2

Ludlow A. D., Navarro J. F., Springel V., Jenkins A., Frenk C. S., Helmi A., 2009, *ApJ*, **692**, 931

Ludlow A. D., Schaye J., Schaller M., Richings J., 2019a, *MNRAS*, **488**, L123

Ludlow A. D., Schaye J., Bower R., 2019b, *MNRAS*, **488**, 3663

Ludlow A. D., Schaye J., Schaller M., Bower R., 2020, *MNRAS*, **493**, 2926

Ludlow A. D., Fall S. M., Schaye J., Obreschkow D., 2021, *MNRAS*, **508**, 5114

Mamon G. A., Sanchis T., Salvador-Solé E., Solanes J. M., 2004, *A&A*, **414**, 445

Marinacci F., et al., 2018, *MNRAS*, **480**, 5113

McCarthy I. G., Schaye J., Bird S., Le Brun A. M. C., 2017, *MNRAS*, **465**, 2936

Naiman J. P., et al., 2018, *MNRAS*, **477**, 1206

Nelson D., et al., 2018, *MNRAS*, **475**, 624

Nelson D., et al., 2019, *Computational Astrophysics and Cosmology*, **6**, 2

O’Neil S., Barnes D. J., Vogelsberger M., Diemer B., 2021, *MNRAS*, **504**, 4649

O’Neil S., Borrow J., Vogelsberger M., Diemer B., 2022, *MNRAS*, **513**, 835

Pedregosa F., et al., 2011, *Journal of Machine Learning Research*, **12**, 2825

Pillepich A., et al., 2018a, *MNRAS*, **473**, 4077

Pillepich A., et al., 2018b, *MNRAS*, **475**, 648

Pillepich A., et al., 2019, *MNRAS*, **490**, 3196

Planck Collaboration et al., 2016, *A&A*, **594**, A13

Ragone-Figueroa C., Granato G. L., Murante G., Borgani S., Cui W., 2013, *MNRAS*, **436**, 1750

Ragone-Figueroa C., Granato G. L., Ferraro M. E., Murante G., Biffi V., Borgani S., Planelles S., Rasia E., 2018, *MNRAS*, **479**, 1125

Sanchis T., Mamon G. A., Salvador-Solé E., Solanes J. M., 2004, *A&A*, **418**, 393

Schaye J., et al., 2015, *MNRAS*, **446**, 521

Simpson C. M., Grand R. J. J., Gómez F. A., Marinacci F., Pakmor R., Springel V., Campbell D. J. R., Frenk C. S., 2018, *MNRAS*, **478**, 548

Somerville R. S., Davé R., 2015, *ARA&A*, **53**, 51

Springel V., 2011, in *Computational Star Formation*. pp 203–206, doi:[10.1017/S1743921311000378](https://doi.org/10.1017/S1743921311000378)

Springel V., Hernquist L., 2003, *MNRAS*, **339**, 289

Springel V., et al., 2005, *Nature*, **435**, 629

Springel V., et al., 2018, *MNRAS*, **475**, 676

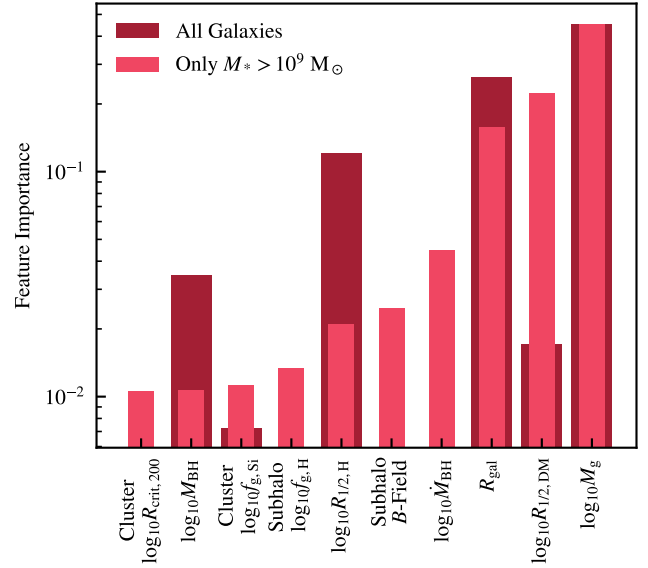


Figure A1. Same as Fig. 6, but only including galaxies with $M_* > 10^9 M_\odot$ in the training set. We see very similar important features, notably the gas mass, distance from cluster centre, and dark matter half-mass size. In the background, in the original red, we show the top 10 feature importances as displayed in the original figure.

Tonnesen S., Bryan G. L., 2009, *ApJ*, **694**, 789

Tremmel M., Karcher M., Governato F., Volonteri M., Quinn T. R., Pontzen A., Anderson L., Bellovary J., 2017, *MNRAS*, **470**, 1121

Tremmel M., Wright A. C., Brooks A. M., Munshi F., Nagai D., Quinn T. R., 2020, *MNRAS*, **497**, 2786

Trujillo I., 2021, *Nature Astronomy*, **5**, 1182

Van Rossum G., Drake Jr F. L., 1995, *Python reference manual*. Centrum voor Wiskunde en Informatica Amsterdam

Virtanen P., et al., 2020, *Nature Methods*, **17**, 261

Vogelsberger M., Genel S., Sijacki D., Torrey P., Springel V., Hernquist L., 2013, *MNRAS*, **436**, 3031

Vogelsberger M., et al., 2014a, *MNRAS*, **444**, 1518

Vogelsberger M., et al., 2014b, *Nature*, **509**, 177

Vogelsberger M., et al., 2018, *MNRAS*, **474**, 2073

Vogelsberger M., Marinacci F., Torrey P., Puchwein E., 2020, *Nature Reviews Physics*, **2**, 42

Weinberger R., et al., 2017, *MNRAS*, **465**, 3291

Weinberger R., et al., 2018, *MNRAS*, **479**, 4056

Weinberger R., Springel V., Pakmor R., 2020, *ApJS*, **248**, 32

Wiersma R. P. C., Schaye J., Smith B. D., 2009, *MNRAS*, **393**, 99

de los Rios M., Martínez H. J., Coenda V., Muriel H., Ruiz A. N., Vega-Martínez C. A., Cora S. A., 2021, *MNRAS*, **500**, 1784

van Dokkum P. G., Abraham R., Merritt A., Zhang J., Geha M., Conroy C., 2015, *ApJ*, **798**, L45

van den Bosch F. C., 2017, *MNRAS*, **468**, 885

van den Bosch F. C., Ogiya G., 2018, *MNRAS*, **475**, 4066

van den Bosch F. C., Ogiya G., Hahn O., Burkert A., 2018, *MNRAS*, **474**, 3043

APPENDIX A: FEATURE IMPORTANCE AT HIGHER MASSES

In Fig. A1, we show the results of our machine learning pipeline from Section 4, applied to galaxies with a stellar mass $M_* > 10^9 M_\odot$ only, to test how our results change when considering what would be typically considered ‘well resolved’ galaxies only. The important features are nearly identical to those when we train the pipeline on

all substructures as in Fig. 6, with the only major missing important feature the stellar half-mass sizes. This is expected, as demonstrated in Fig. 10, the differences in stellar profiles were mainly powered by the lowest-mass galaxies and were only marginally resolved in the TNG-300 simulation.

The black hole mass feature is replaced with the black hole accretion rate, but again this is simply used for occupation checking. The final, somewhat important, feature that is new here is the Subhalo B -field. This feature is somewhat degenerate with the gas mass, with backsplash haloes that retain gas having relatively low magnetic field strengths due to their low gas fraction.

As the same qualitative trends remain from our main results, and there are potentially interesting features shown in the $10^8 < M_*/M_\odot < 10^9$ mass range, in the main text we retain the larger sample.

This paper has been typeset from a $\text{\TeX}/\text{\LaTeX}$ file prepared by the author.